# Introduction to computed tomography

**Cantatore, Angela; Müller, Pavel**

*Publication date:*
2011

*Document Version*
Publisher's PDF, also known as Version of record

# Introduction to computed tomography

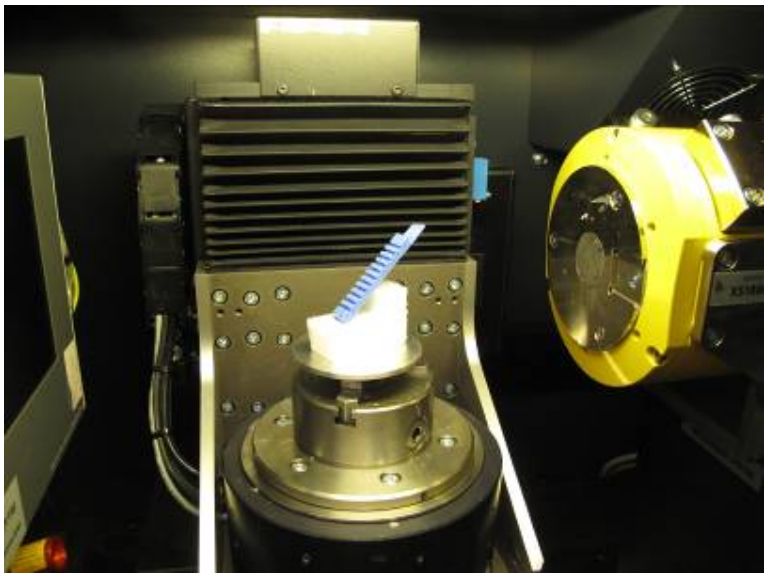

Angela Cantatore

Pavel Müller

March 2011

**Manufacturing Engineering**
Department of Mechanical Engineering
Technical University of Denmark

## Foreword

Since computed tomography (CT) has entered the industrial environment around thirty year ago, an increasing interest for this technology was shown especially in the non-destructive testing, thanks to its advantages in comparison with traditional destructive techniques. The development of powerful systems with more stable X-ray sources and better detectors aroused the interest of manufacturing and coordinate metrology. The current challenges of CT is in the quantification of measurement uncertainty, which is not fully established yet because of multiple factors affecting the traceability of these systems.

This report is an initiative of the project "Center for the industrial application of CT scanning - CIA CT: Advanced 3D scanning measurement, quality assurance and product development in industry". The four-year CIA-CT project is promoted by a consortium constituted by nine companies having expertise in the CT field in Denmark with the aim of creating a national competence center in the industrial application of CT and conduct research of benefit to the participating firms, Danish industry and Danish society, focusing on the industrial application of CT as advanced 3D scanning measurement, quality assurance and product development.

This report focuses on CT applications for industrial and metrological purposes, where attention is on the current challenges in CT, i.e. establishment of traceability and uncertainty assessment. An overview of factors influencing CT accuracy is described. A thorough review of the state of the art, a theoretical analysis and an experimental investigation in order to assess the influence of reference, instrument, workpiece, environment and procedure on the precision and traceability of measurement results from CT, is realized. In particular, experimental investigations concern methods and techniques to correct and reduce errors and artefacts due to a defined parameter, both as they can be found in literature and performed by the authors.

*Angela Cantatore, Pavel Müller*

# Contents

# Chapter 1

# Introduction

This chapter provides a short introduction to computed tomography (CT), covering the main milestones from the discovery of X-ray till modern applications of CT in the field of industrial metrology.

## 1.1 State of the art

X-rays were discovered in 1895 by the German physicist Wilhelm Conrad Röntgen, who earned the Nobel Prize in Physics in 1901. Although their potential applications in medical imaging diagnosis were clear from the beginning, the implementation of the first X-ray computed tomography system was made in 1972 by Godfrey Newbold Hounsfield (Nobel prize winner in 1979 for Physiology and Medicine), who constructed the prototype of the first medical CT scanner and is considered the father of computed tomography. CT was introduced into clinical practice into 1971 with a scan of a cystic frontal lobe tumor on a patient at Atkinson Morley Hospital in Wimbledon (United Kingdom). After this, CT was immediately welcomed by the medical community and has often been referred to as the most important invention in radiological diagnosis, since the discovery of X-rays [1].

The first applications of CT in an industrial context is traced back to the first 1980´s, in the field of non destructive testing, where small number of slices of the object were visually inspected. 3D quantitative industrial CT applications appeared in the later 1990s, with simple volume and distance analysis [2]. Today, thanks to relevant improvements in both hardware and software, CT has become a powerful and widely used tool among non destructive techniques, capable of inspecting external and internal structures (without destroying them) in many industrial applications. Development of more and more stable X-ray sources and better detectors led to design of more complex CT system, providing accurate geometrical information with micrometer accuracy. CT is widely used for geometrical characterization of test objects, material composition determination, density variation inspection etc. In a relative short time, CT is capable to produce a complete three-dimensional model and tolerances of the scanned machined parts can be verified.

Because of the growing interest on precision in production engineering and an increasing demand for quality control and assurance, CT is leading the field of manufacturing and coordinate metrology. With respect to traditional techniques, CT systems have

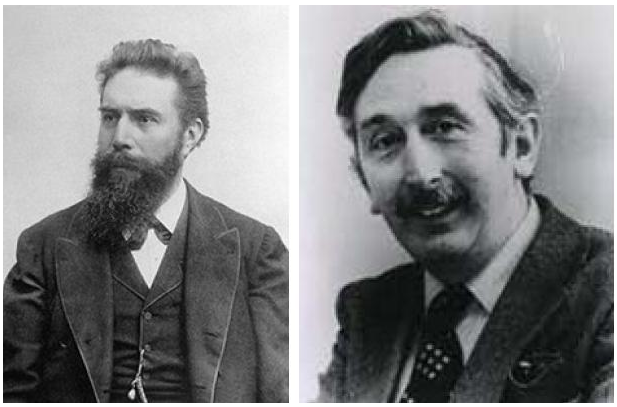

Figure 1.1: *A picture of Wilhelm Conrad Röntgen (27 March 1845 – 10 February 1923) (left), and Godfrey Newbold Hounsfield (28 August 1919 – 12 August 2004), (right) [3, 4].*

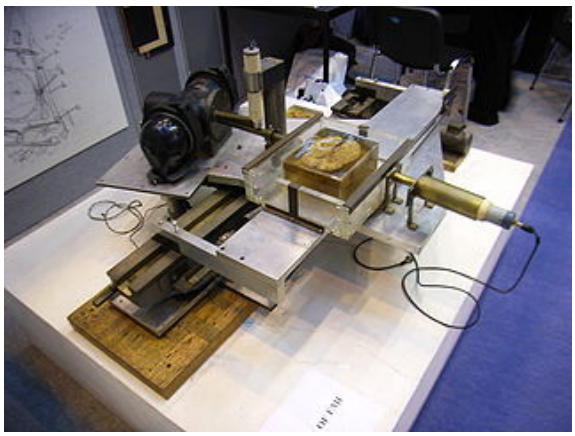

Figure 1.2: *First CT scanner prototype developed by Hounsfield [5].*

indisputable advantages: internal and external geometry can be acquired without destroying the part, with a density of information much higher than common tactile and optical coordinate measuring. A key parameter for reliability of the measurement process is the establishment of measuring uncertainty. Since there are many influence parameters in CT, uncertainty contributors in CT and standards dealing with quantification of CT have not been completely established yet. The assessment of the uncertainty budget becomes a challenge for all researchers.

## 1.2 Structure of the report

The general purpose of this report is to give a general introduction to computed tomography (CT). This report presents state of the art in CT and discuss preliminary investigations performed by the authors. It is divided into several chapters discussing various topics concerning CT. The content of individual chapters is briefly described in the following points:

- From discovery of X-rays to high quality dimensional measurements

- Selected methods of non-destructive testing of materials (Chapter 2)
- Description of CT technology in general, including the principal of CT, comparison between medical and industrial CT systems, classification of CT systems, their applications and advantages and disadvantages (Chapter 3)
- Description of influence factors in CT, state of the art, theoretical analysis and preliminary experimentation on some influence factors performed by the authors (Chapter 4)

# Chapter 2

# Non-destructive testing

Industrial CT is referred to so-called NDT technologies. "Non-destructive testing" collects all methods and techniques for product quality assurance and inspection without destroying the part under investigation. The goal of these methods is to analyze the integrity of a material, component or structure and quantitatively measure some characteristics of the product in many different industrial applications. Due to two main advantages with respect to destructive methods (being less expensive and less time-consuming) they are widely applied methods in the industrial environment.

Besides CT, there are different inspection methods used for specific tasks. In the following, some of them will be briefly presented. CT will be treated widely in the following chapters.

## 2.1 Magnetic part inspection

This method is used to detect surface (or close to surface) defects, mainly in ferromagnetic materials like steel and iron. The basic principle is shown in Figure 2.1. A magnetic flux is generated in the part under analysis. If there is a defect, like a crack, the magnetic flux will leak and the crack edge will work as a magnetic attractive pole. So by applying for example particles of iron, they will be attracted toward the defect, indicating it. Main advantage and disadvantages are reported in Table 2.1.

Table 2.1: Advantages and disadvantages of magnetic part inspection [6].

| **Advantages** | **Disadvantages** |
|---|---|
| • Simplicity of operation | • Only for ferromagnetic materials |
| • Quantitative | • Only for surface-near surface defects |
| • Can be automated | • Impossibility to characterize depth and orientation of defects |

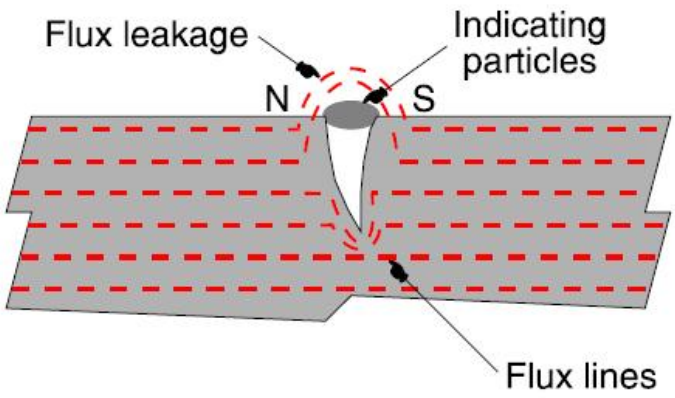


Figure 2.1: *Principle of magnetic particle inspection [6].*

Table 2.2: Advantages and disadvantages of magnetic part inspection [6].

| **Advantages** | **Disadvantages** |
|---|---|
| • Simplicity of operation | • Only for ferromagnetic materials |
| • Quantitative | • Only for surface-near surface defects |
| • Can be automated | • Impossibility to characterize depth and orientation of defects |

## 2.2 Eddy current testing

The eddy current testing is used to detect little cracks and defects on or near-surface of the material and to measure coating thickness in an electrically conducting material (such as stainless steel, aluminum).

The method exploits the principle of the electromagnetic induction: eddy currents are produced in any electrically conducting material that is subjected to an alternating magnetic field, generated by a coil. Presence of a discontinuity on the surface (like a crack) of the material causes a change in the coil impedance, which can be measured and correlated with the cause of the modification. Coils can also be used in pair to enhance the signal [6, 7]. Figure 2.3 shows a picture of a crack in a stainless steel disc obtained with eddy current. Main advantages and disadvantages of eddy current testing are reported in Table 2.3.

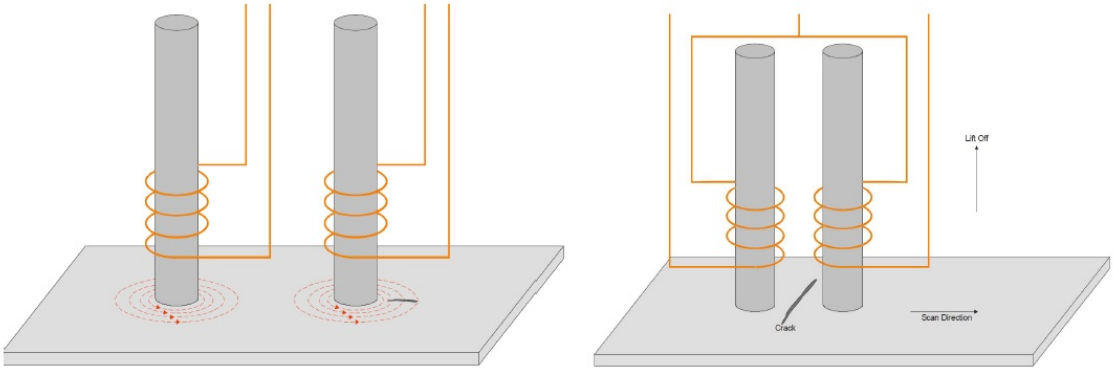


Figure 2.2: *Principle of eddy current. Coil with single winding (left), and coil with two windings (right) [6].*

Table 2.3: Advantages and disadvantages of eddy current testing [6, 7].

| **Advantages** | **Disadvantages** |
|---|---|
| • Suitable for determining a wide range of condition of the material (presence of defects, composition, hardness, conductivity, etc.) | • Only for electrically conducting (metallic) materials |
| • Information can be provide in a simple way | • Maximum inspectable thickness is approx. 6 mm |
| • High inspection speeds possible | • Inspection of ferromagnetic materials is difficult using conventional eddy current tests |
| • Extremely compact and portable unit are available | • Operator skilled required |
| • Suitable for hugh automation | • Use of calibration standards necessary |

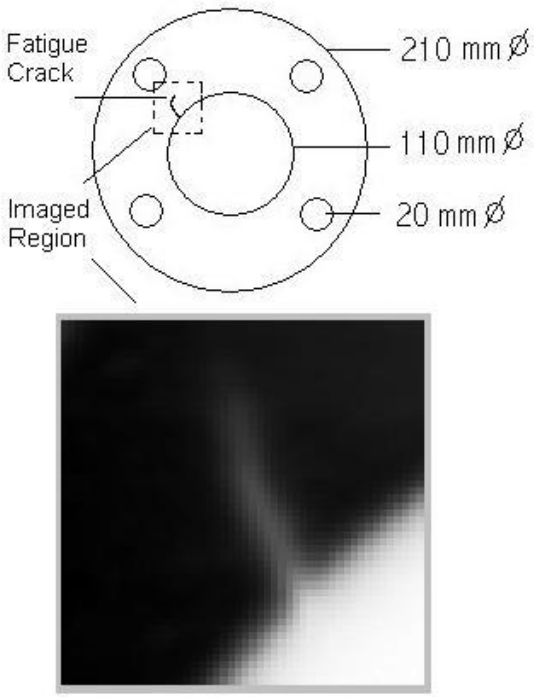


Figure 2.3: *Grey level image of a fatigue crack of a stainless steel disc obtained with eddy current [7].*

## 2.3 Ultrasonic testing

This method is used to detect defects at the surface and internal (in depth) to sound conducting materials. There are two methods of receiving the ultrasound waveform, ”pulse echo” and ”through transmission”. In pulse echo systems, a short pulse of ultrasound is generated by the transducer (usually a piezo electric crystal) and sent into the material. The energy passes into the material, reflects from the back surface, and is detected by the same transducer, yielding a signal on an oscilloscope with a time base. The transducer performs both the sending and the receiving of the pulsed waves from and back to the device. Reflected ultrasounds come from an interface, such as the back wall of the object or from an imperfection within the object. The oscilloscope normally shows the original pulse of the ultrasonic transducer (front surface echo), the back reflection and any extra blip indicating a reflection from a defect in the material. From the oscilloscope timing, the depth of the defect below the surface can be determined. In through-transmission systems, a transmitter and receiver unit are separate and placed at opposite sides of the test object. Imperfections or other conditions in the space between the transmitter and receiver are sensed as a reduction of intensity of ultrasonic energy by the receiving unit, thus revealing their presence [7]. Ultrasonic testing can also be used to detect defects that are not plane oriented but with an angle with respect of the test surface. Figure 2.4 shows an example of defect detection in steel part using a normal probe (left) and an example of detection of angled defect in weld inspection using an angle probe. Main advantages and disadvantages of this technology are listed in Table 2.4.

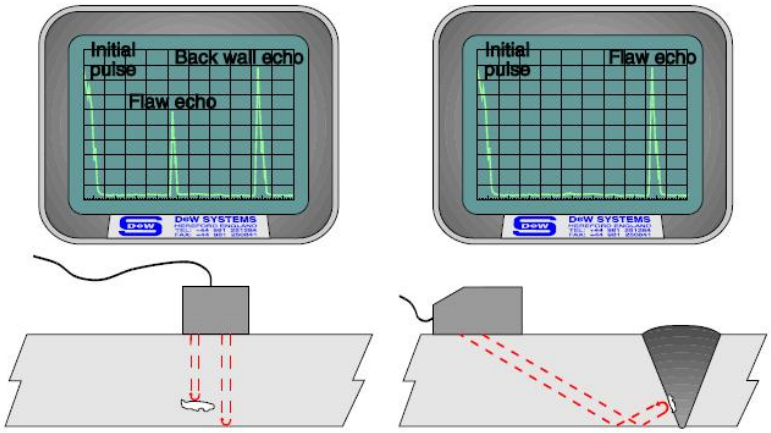


Figure 2.4: *Example of defect detection through ultrasonic testing, using a normal probe (left) and an angle probe for detection of imperfections with an angle with respect to the test surface (right) [6].*

Table 2.4: Advantages and disadvantages of ultrasound testing [6].

| **Advantages** | **Disadvantages** |
|---|---|
| • Thickness and length up to 9 m can be tested | • Indication requires interpretation |
| • Extremely sensitive | • Difficulties with very thin surfaces |
| • Capable of being fully automated | • Skills required to gain the fullest |
| • No consumable | information from the test |
| | • Limited resolution |

## 2.4 Optical non-destructive testing

Optical NDT collects all methods that works by illuminating the object surface with light and examining the reflected light patterns using visualization systems. These methods are widely applied in surface analysis for the detection and study of crack propagation, study of corrosion and deformation analysis and are regarded as the most effective and least expensive among the NDT techniques [7]. Different systems can be found but two of the most used are holographic interferometry and electronic speckle pattern interferometry.

### 2.4.1 Holographic interferometry

Holographic interferometry is used to measure "displacements" (such as it occurs dealing with stress, strain, vibrations) and for other NDT applications (defects analysis, imperfections analysis, residual stress, etc.). The technique works on the basis of holography (see Figure 2.5): the light coming from a laser (coherent light source) is split in two beams: one of it illuminates the object under testing and the other one is used as a reference. At the recording site, from the interference path originated between the light reflected by the object and the reference beam it is possible to reconstruct the 3D picture of the object. In holographic interferometry, the system records the two complete wave patterns coming from the objects in its original position (taken as a reference) and in deformed states [8]. The combination of these two wave patterns originates an

interference fringe pattern, called interferogram, related to the movement that has taken place. The contours of equal displacement are mapped by the fringes with approximately one-half the wavelength of the light source [9]. An example is showed in Figure 2.6.

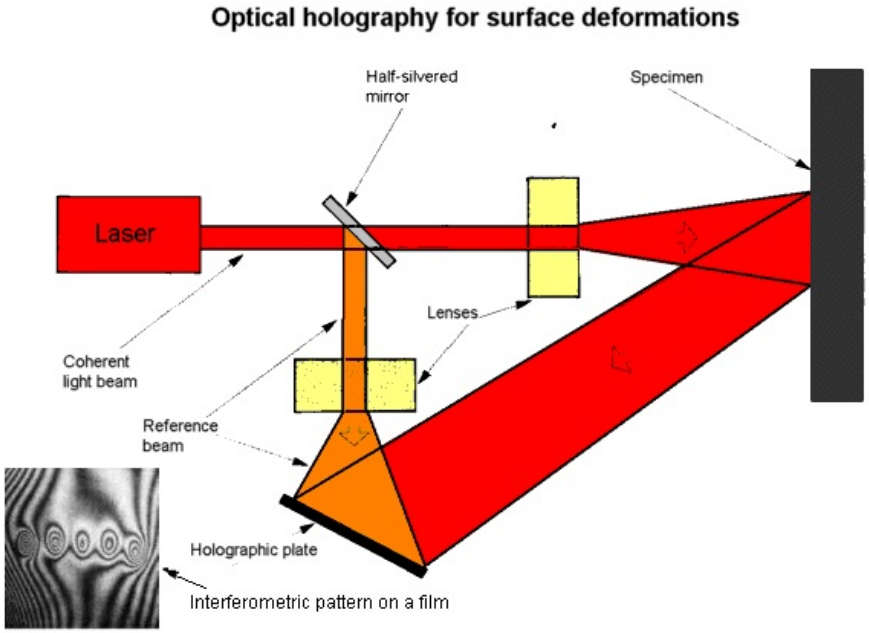


Figure 2.5: *Principle of optical holography [10].*

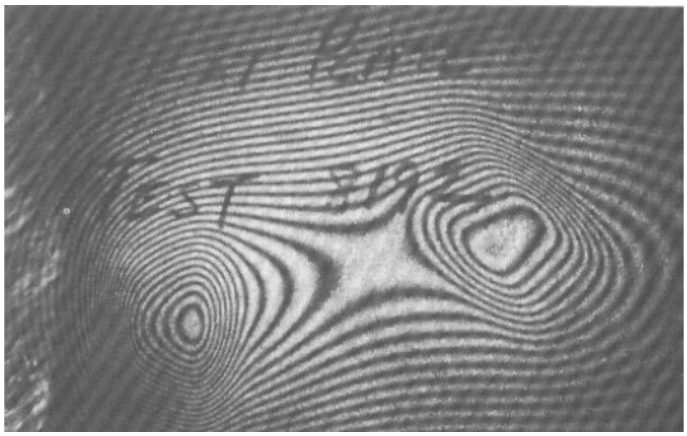

Figure 2.6: *Double exposure hologram of a stressed flat metal plate [11, 12].*

### 2.4.2 Electronic speckle pattern interferometry

Electronic speckle pattern interferometry is based on the ”speckle phenomenon”. It is a random intensity pattern produced by the interference between the light rays (from a coherent source as a laser beam) as they are scattered by different points on a rough

surface. The visual result is a grainy image of the illuminated surface. Electronic speckle pattern interferometry produces an output similar to holographic interferometry: a fringe pattern is generated from the interference between the speckle pattern formed by the illuminated surface of the object to be tested and a reference wave. This fringe pattern is stored as an image and when the object is deformed or moved, the resultant speckle pattern changes, due to the change in path difference between the wavefront from the surface and the reference wave. This second speckle pattern is transferred to the computer and subtracted from, or added to, the previously stored pattern. The resulting interferogram is then displayed as a pattern of dark and bright fringes, called correlation fringes, as the fringes are produced by correlating the intensities of the resultant speckle patterns taken before and after displacement [9]. Two example are shown in Figure 2.7.

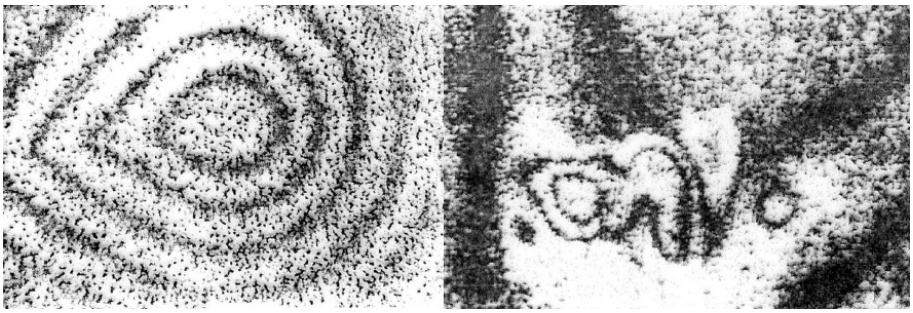

Figure 2.7: *Longitudinal crack in a steel welding (left); Delamination in a plate (right) [8].*

Main advantages and disadvantages of optical NDT testing in general are reported in Table 2.5.

Table 2.5: Advantages and disadvantages of optical testing [13–15].

| **Advantages** | **Disadvantages** |
|---|---|
| • Non contact measurement | • Indication sometimes requires interpretation |
| • High resolution | • Special safety regulations for laser operation |
| • Full-field information | • Components have to be loaded to see results |
| • No consumable | • Can be applied only for surface or through surface |
| • Real-time measurements | opening |

Figure 2.8 shows the classification of chosen NDT techniques (including CT) according to their penetration depth and their spatial resolution. From this table it is possibile to assess efficacy of the method in material defect detection. Optical interferometry achieves the highest resolution but they can basically monitor surfaces or coatings. In contrast, the best penetration depth combined with a high resolution is usually gained by X-ray CT [16]. Similar conclusions can be drawn from Figure 2.9, where above techniques are classified on the basis of geometrical complexity for dimensional measurements. Here, the emphasis is on the measurement of geometrical parameters, e.g. the geometry of components as compared to constructed (CAD) data [16]. Among NDT methods, CT has the best performances in terms of penetration depth and resolution and this explains many applications of CT in NDT field, as it will be shown in chapter 3.

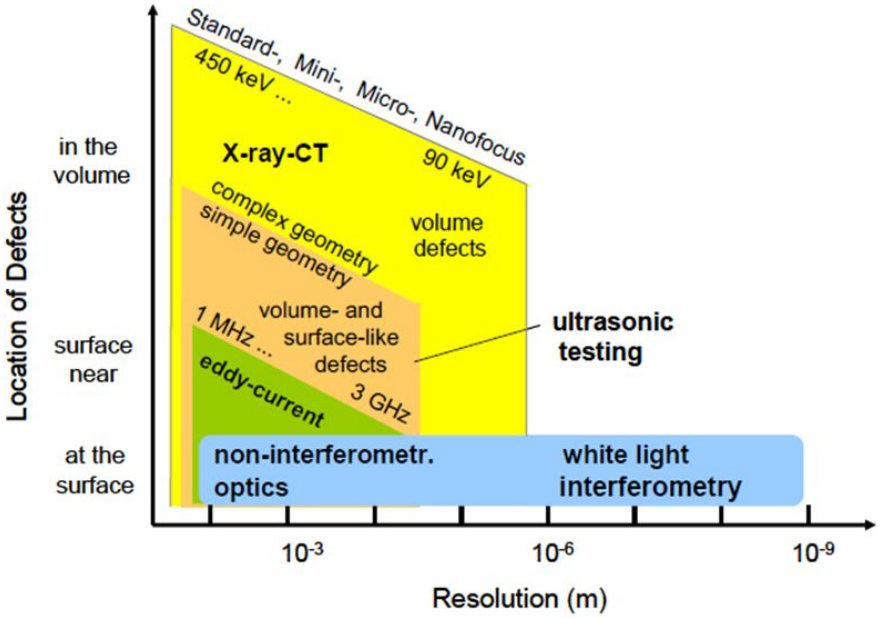


Figure 2.8: *Classification and comparison of chosen NDT techniques and optical measurement techniques according to detectable defect location and spatial resolution [16].*

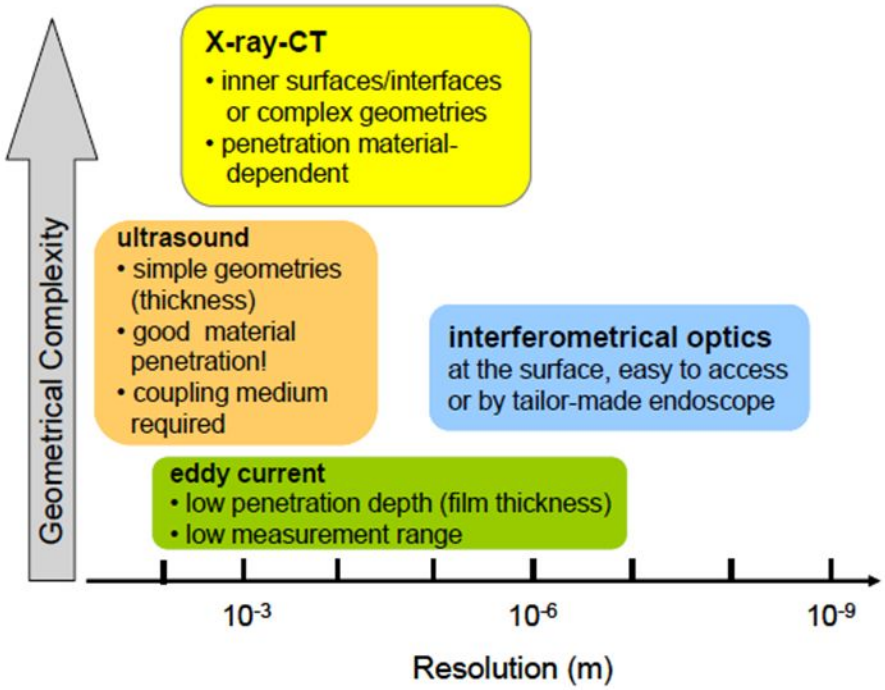


Figure 2.9: *Classification of chosen NDT techniques according to geometrical complexity and resolution [16].*

# Chapter 3

# CT technology

CT is a powerful tool capable of inspecting external and internal structures in many industrial applications as well as providing accurate geometrical information with very high accuracy. This chapter describes principle of CT, pointing out the main difference between medical and industrial CT scanners, classification of CT systems, applications of CT as a tool used in industry as well as a powerful tool used in coordinate metrology. Lastly, advantages and disadvantages of the use of CT are presented.

## 3.1 CT principle

A CT system consists of an X-ray sourceÂ, a rotary table, an X-ray detector and a data processing unit for computation, visualization and data anlysis of measurement results (see Figure 3.1).

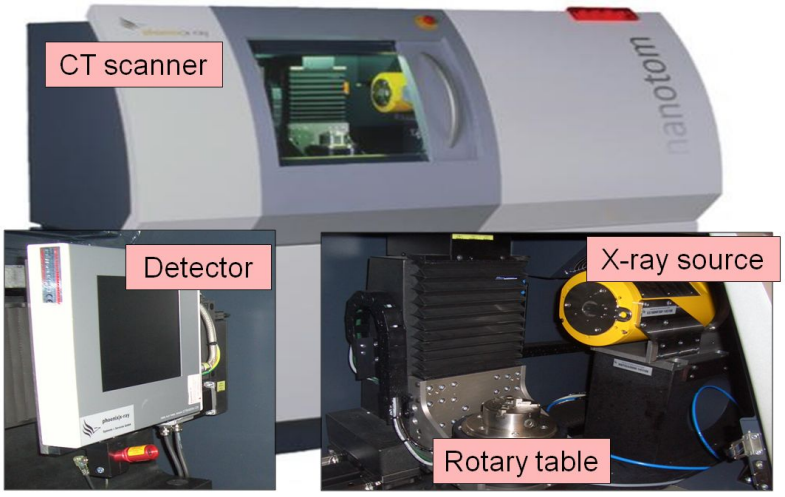


Figure 3.1: *Industrial cone beam CT scanner [GE Phoenix|X-ray Nanotom].*

In principle, CT creates cross section images by projecting a beam of emitted photons through one plane of an object from defined angle positions performing one revolution. As the X-rays (emitted photons) pass through the objectÂ, some of them are absorbedÂ, some are scatteredÂ, and some are transmitted. The process of X-ray intensity reduction,

involving just those X-rays which are scattered or absorbed, is called attenuation. X-rays which are attenuated due to the interactions with the object do not reach the X-ray detector. Photons transmitted through the object at each angle are collected on the dectector and visualized by computer, creating a complete reconstruction of the scanned object. The 3D gray value data structure gained in this way represents the electron density distribution in the measured object [17].

A process chain, that is the way a measurement result is obtained, including four different measuring tasks are described in a draft of a German guideline VDI/VDE 2630 part 1.2 [18]. A general process chain is presented in Figure 3.2 and described as follows:

1. Firstly, the acquisition (scanning) of an object is performed. Several parameters have to be set prior to scanning, e.g. magnification, orientation of the object, energy of the X-ray source, detector integration time etc.

2. After scanning and obtaining a set of 2D projections, the volume is reconstructed. The volume is modeled as a 3D matrix of voxels (abbreviation for volumetric pixels), where each voxel value represents the corresponding local attenuation coefficient of the scanned object. In other words, to each voxel a gray value is assigned representing a local X-ray absorption density. Here, some correction techniques can be applied on the 2D projections in order to minimize the effect of scattered radiation and beam hardening (more about influence factors is mentioned in Chapter 4).

3. Then, the threshold value has to be carefully determined as it is a critical parameter for accurate image segmentation and surface data determination, thus has a great influence on the final geometry [19] (more about threshold is discussed in Section 4.2.2).

4. After a threshold value is determined, either the surface data or volume data are generated. Surface data are generated in the STL format, characterized by a polygonal mesh in the shape of triangles, on the surface.

5. Then, direct dimensional measurement (e.g. fitting of geometrical primitives, wall thickness analysis, nominal/actual comparison) can be performed on either of the earlier mentioned data sets (volume / surface).

6. Finally, a measurement result is obtained.

There are two main CT systems which can be found in industry. These are: (1) 2D-CT (see Figure 3.3(a)), and (2) 3D-CT (see Figure 3.3(b)). 2D-CT systems have a fan beam source and a line detector which enable the acquisition of a slice of a 3D object by coupling a translation and rotation movement of the object. This sequence of rotation and translation is repeated depending on number of slices which have to be reconstructed. The main drawback of these systems is the long scanning times (especially when working with big parts). This problem is overcome by 3D-CT systems. The system consists of a flat area detector and a cone beam source, enabling the acquisition of a slide of the object just with one revolution of the rotary table. No linear translation of the rotary table is needed. This solution allows significant improvement in acquisition time but, on the other hand, other problems arise due to the cone beam source. Scattered radiations and reconstruction

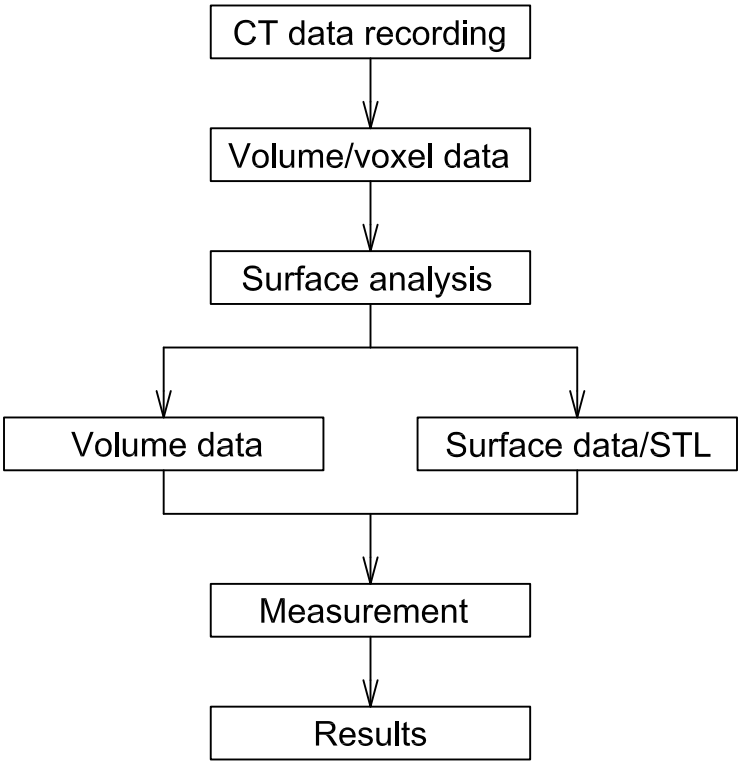


Figure 3.2: *Process chain for CT measurement.*

artefacts at the top and bottom of the geometry can affect the quality of the reconstructed geometry. In particular, scanning quality deteriorates from the center to the borders of the detector, because of geometrical reasons [20]. An example is shown in Figure 3.4, where it can be seen that more noise is present at the border of the scanned sample. The most recent evolution of 3D-CT is represented by systems exploiting a helical scan geometry, where rotation of the object is simultaneously performed with a translational movement along the rotation axis [20, 21], see Figure 3.5. The advantages of this solution are two. In first instance, there are no restrictions on the sample length (along the rotation axis direction); the helical trajectory can be prolonged for object bigger than detector dimension and theoretically object of unlimited length can be reconstructed. In second instance, with an appropriate shift of the part, a bigger number of slices of the object will be projected in the middle part of the detector, leading to a more complete acquisition, and so to a constant resolution along the rotation axis. In this way also top and bottom areas will be scanned with the same resolution as the central one. An example is shown in Figure 3.6, where a pen scanned using both a typical CT scanner and a helical CT scanner. While in the first case resolution at the bottom part is not easy to distinguish single ribs, the helical CT enables to scan the whole geometry (top, central and bottom part of the object) with the same quality [20].

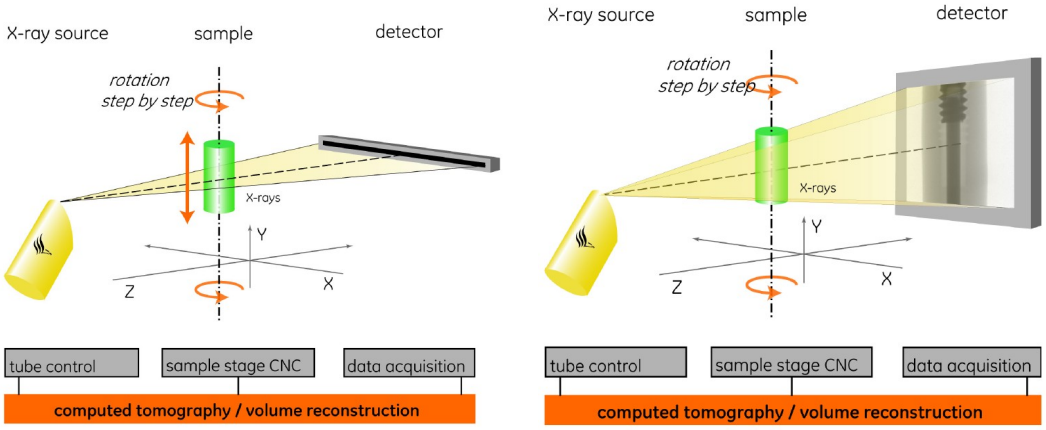


(a) *2D-CT using line detector.* (b) *3D-CT with flat panel detector.*

Figure 3.3: *CT scanner principal [Source: Phoenix|X-ray].*

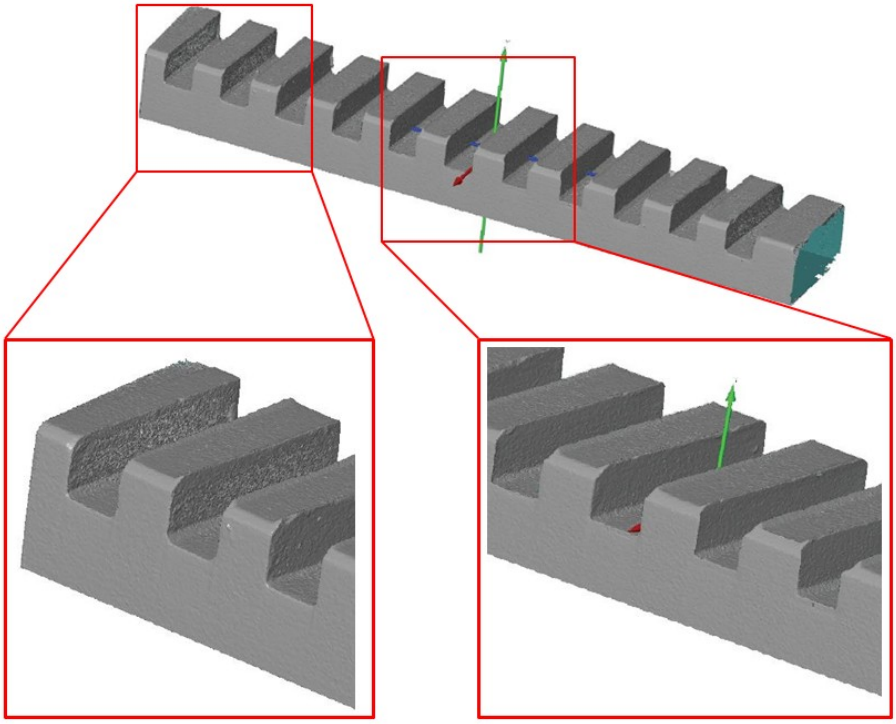

Figure 3.4: *Scanning of a replica step gauge: artefacts in cone beam CT.*

## 3.2 Medical vs. Industrial CT systems

It is known that CT scanners were first used for medical purposes. The main difference in the setup of industrial and medical CT systems is that in the case of industrial CT, the object rotates on a rotary table and the X-ray source is steady, whereas in medical CT, the X-ray sources rotate and the object (a human body in the most cases) is lying on a table/bed which is steady. Schematic principal and example of medical and industrial

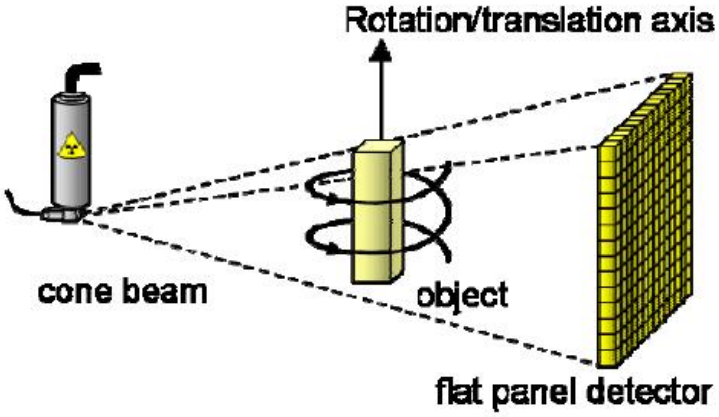


Figure 3.5: *Helical CT geometry [20].*

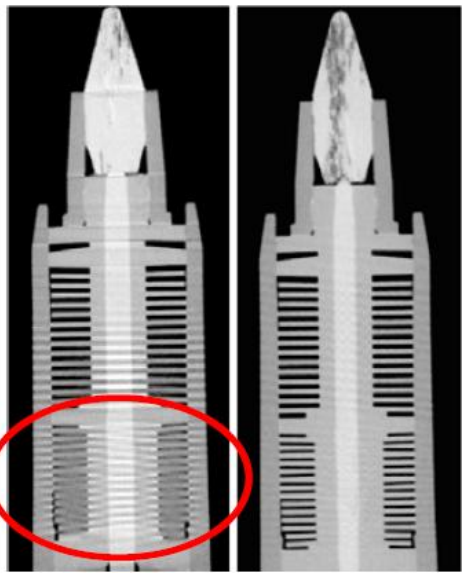

Figure 3.6: *Comparison between a scan obtained with a cone beam CT and helical CT of a pen [20].*

CT scanners is shown in Figure 3.7. Other important comparisons of the two types of scanners embody in:

- Material type (tissue, blood and bone for medical and polymers, wood, concrete, ceramics, metals and composites for industrial CT scanners)
- Applied energy (<200 KeV for medical and up to 15 MeV for industrial CT scanners)
- Achieved resolution of the system (1-2 mm for human subjects in medical and <0.5 mm (macro CT systems) and $10 - 20\ \mu m$ (micro CT systems) for industrial CT systems)

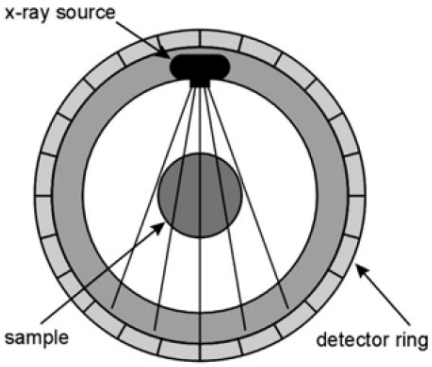


(a) *Principal of a medical CT [22].*

(b) *Example of a medical CT [23].*

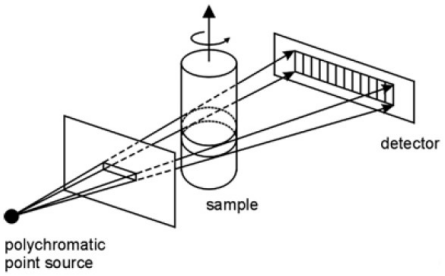


(c) *Principal of an industrial CT [22].*


(d) *Example of an industrial CT [GE Phoenix|X-ray].*

Figure 3.7: *An example of medical and industrial CT scanners.*

**5 generations of medical CT scan geometries**

Figure 3.8 illustrates classification of medical CT scanners. The classification, depending on the scanner geometry, is divided into five generations.

*First-generation*
First-generation CT systems are characterized by a single X-ray source (pencil beam) directing across the object and a single detector. Both, the source and the detector, translate simultaneously in a scan plane. This process is repeated for a given number of angular rotations. The advantages of this design are simplicity, good view-to-view detector matching, flexibility in the choice of scan parameters (such as resolution and contrast), and ability to accommodate a wide range of different object sizes. The disadvantage is longer scanning times.

*Second-generation*
Second-generation CT systems use the same translate/rotate scan geometry as the first generation. The difference here is that a pencil beam is replaced by a fan beam and a single detector by multiple detectors so that a series of views can be acquired during each translation, which leads to correspondingly shorter scanning times. So, objects of wide range sizes can be easily scanned with the second-generation scanners.

*Third-generation*
Third-generation CT systems normally use a rotate-only scan geometry, with a complete view being collected by the detector array during each sampling interval. Typically, third-generation systems are faster than second-generation systems. The detectors here have incorporated bigger amount of sensors in the detector array.

*Fourth-generation*
Fourth-generation CT systems also use a rotate-only scan motion. Here, the system consists of a fixed ring with multiple detectors and a single X-ray source (fan beam) which rotates around the scanned object. The number of views is equal to the number of detectors. These scanners are more susceptible to scattered radiation.

*Fifth-generation*
Fifth-generation CT systems are different from the previous systems, in that there is no mechanical motion involved. The scanner uses a circular array of X-ray sources, which are electronically switched on and off. The sources project on to a curved fluorescent screen, so that when an X-ray source is switched on, a large volume of the part is imaged simultaneously, providing projection data for a cone beam of rays diverging from the source. Here, a series of two-dimensional projections of a three-dimensional object is collected.

A second-generation scan geometry is attractive for industrial applications in which a wide range of part sizes must be accommodated, since the object does not have to fit within the fan of radiation as it generally does with third- or fourth-generation systems. A third-generation scan geometry is attractive for industrial applications in which the part to be examined is well defined and scan speed is important. To date, first-, fourth-, and fifth-generation scan geometries have seen little commercial application [24].

An interesting and valuable review of CT technique, mainly used in the medical area, is presented in [1]. The paper presents and focuses on technology, image quality and clinical applications in chronological order. It also describe a novel use of CT such as dual-source CT, C-arm flat-panel-detector CT and micro-CT.

Because industrial CT systems image only non-living objects, they can be designed to take advantage of the fact that the items being studied do not move and are not harmed by X-rays. They employ the following optimizations:

1. Use of higher-energy X-rays, which are more effective at penetrating dense materials

2. Use of smaller X-ray focal spot sizes, providing increased resolution

3. Use of finer X-ray detectors, which also increases resolution

4. Use of longer integration times, which increase the signal-to-noise ratio and compensate for the loss in signal from the diminished output and efficiency of the source and detectors.

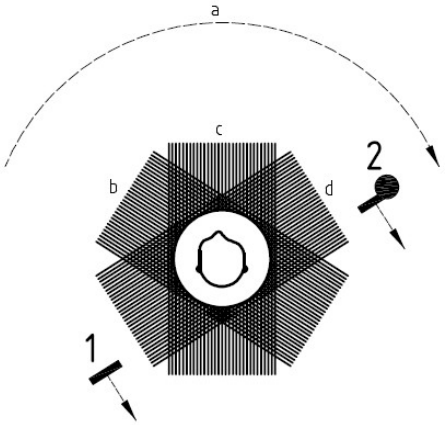


(a) *1st generation single pencil beam translate/rotate scanner.*

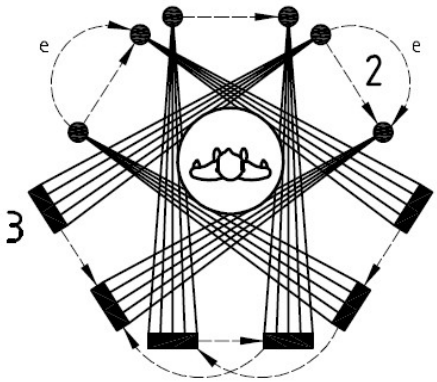


(b) *2nd multiple pencil beam translate/rotate scanner.*

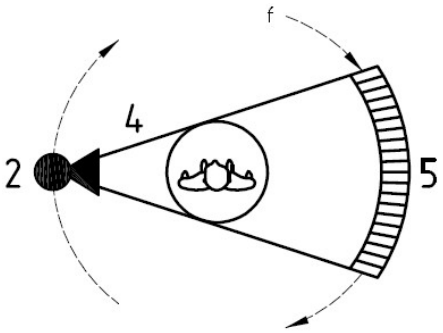


(c) *3rd generation rotate/rotate fan beam scanner.*

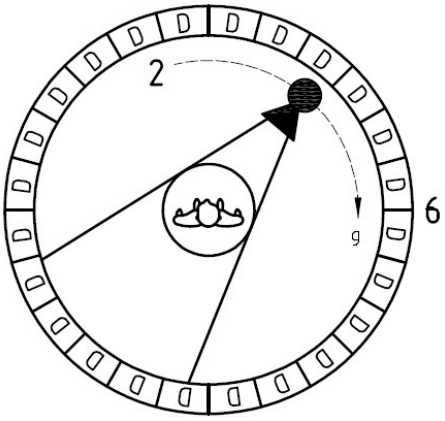


(d) *4th generation rotate/stationary inverted fan beam scanner.*

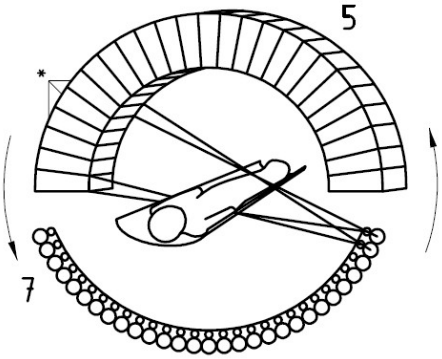


(e) *5th generation cone beam 'cylindrical' scanner.*

Figure 3.8: *Evolution of medical CT scan geometries. 1: detector, 2: X-ray tube, 3: Multiple detectors, 4: Pulsed fan beam, 5: Detector array, 6: Stationary detector array, 7: X-ray source [24].*

## 3.3 CT systems classification

Industrial CT systems can be basically classified into four groups:

1. LINear ACcelerators (LINAC)
2. Macro CT
3. Micro CT
4. Nano CT

The classification of CT systems is based on their achievable resolution, measuring range and spot size. Macro CT systems are used for large and micro CT systems for small measurement objects. Micro CT can be achieved using X-ray tubes with small focal spot sizes (being in the range $1 - 50\ \mu m$) and by positioning the object close to the focus. In this way a higher geometrical magnification is achieved. The resolution of micro CT is limited - among other things - by the size of the focal spot. X-ray sources with nanofocus X-ray tubes (i.e. focal spots smaller than $1\ \mu m$) are the most appropriate for scanning objects of smaller size. Figure 3.9 shows achievable resolution versus measuring range. It is clear that scanning smaller parts enhances to achieve smaller resolution.

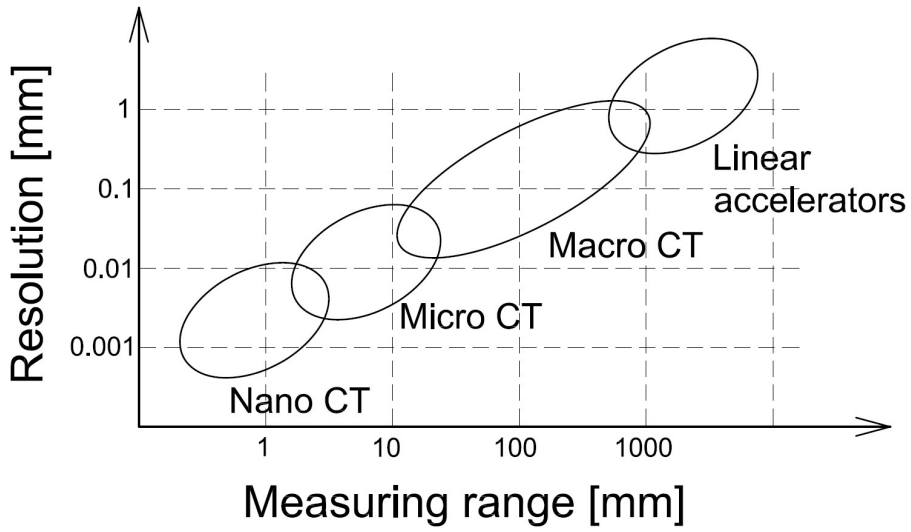


Figure 3.9: *Achievable resolution vs. measuring range. Adapted from [25].*

## 3.4 CT applications

The main interest for the industrial application of CT is, as mentioned in Chapter 1, the non-destructive analysis of faults (e.g. cracks or shrink holes) and the material composition inside the volume of the scanned part. The latter is mainly used in the automotive industry for big casting's inspection and quality control of engine blocks, gear boxes and other mechanical samples. CT is able to detect density variations within

the percent range. Hence, qualitative statements on material defects can be made. Thanks to improved technology, industrial CT is now being developed towards a quantitative inspection technique. Thus, current CT systems are not only able to detect defects, but can also make statements about the size and distribution of these defects [17]. Among other important industrial applications belong first article inspection which is important to detect weaknesses of the product in its early stage and therefore increase productivity of the process.

Since CT data contain a complete volumetric information about the measured body, it is possible, by generating surfaces on the scanned volume, to determine coordinates of the measured body. This means that CT can be used to perform dimensional measurements like coordinate measuring machines (CMMs). Since some years CT is increasingly used in industry for dimensional measurements. Applications/measuring tasks are focused here on the absolute determination of geometrical features like wall thicknesses or on the comparison of the measured geometry with reference data sets. In most cases nominal CAD data of the part are used as reference [26]. The latter is done after registration of both actual and nominal geometries and allow to display a 3D variance map (color map). CT finds its use in many different industrial fields, such as:

- Material science
- Electronics
- Military
- Medical / food
- Archeology
- Security
- Aerospace
- Automotive

The main CT applications are presented in Table 3.1. As it was mentioned above and in Chapter 2, Table 3.1 is divided into two categories, NDT and metrology.

Table 3.1: CT applications.

| **NDT** | **Metrology** |
|---|---|
| • Defect/failure analysis | • CAD comparison |
| • Crack detection and measurement | • Nondestructive internal |
| • Assembly inspection | measurements |
| • Porosity and void detection and analysis | • Reverse engineering |
| • Density discrimination - material | • 3D volume analysis |
| composition | • First-Article Inspection (FAI) |

The authors would like to point out one important problem which can occur when comparing the CT data with the CAD data. It is disputable whether the variances in the CT data set are due to the inaccuracies in the manufacturing process or due to the CT

data itself. Therefore, it is highly recommended to compare the CT measurements with measurements performed on the optical instrument or even better on the CMM, where the measuring uncertainty is known. This problem was also described in [27]. Second disputable problem appears when the CT data points are compared with the CMM data points. It is very important to choose the correct measuring strategy when both data sets are compared. This means, that for direct comparison of both data sets, is recommended to compare exactly the same points on the object, that means to select the same points on the CT point cloud as were the probed points by the CMM. This was pointed out by Dr. Oliver Brunke on High Resolution X-ray CT Symposium in Dresden [28]. It was found, that differences can be in the order of several micrometers. The problem concerning measuring and evaluation strategy is being part of the ongoing research at DTU.

Some of the applications of CT used in above mentioned industrial fields are described for example in [25], provided by Phoenix|X-ray, or in [29] presented at the 14th CMM Danish users club conference on Applications of CT CT in industry at DTU. However, to show a reader some examples of CT applications, these are illustrated below.

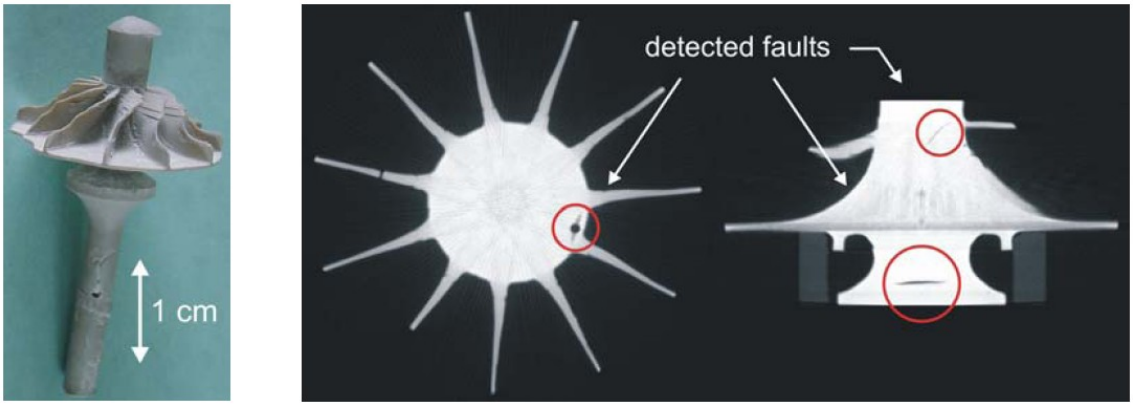


Figure 3.10: *Detection of faults on a micro turbine; left: Photography; right: Slice images achieved by CT [26]*

## 3.5 Advantages and disadvantages

As presented earlier in this chapter, CT brings multiple advantages, but as one will realize later on, also numerous disadvantages. One of the main advantages is the fact that CT is being used more and more in the industrial word for non-destructive testing of products. In the field of metrology, this non-contact technology helps to measure inner and outer features within very short acquisition time precisely, without destroying the item. A CT scan consists of a data set of a huge amount of measuring points. Any other measuring instrument cannot acquire such big amount number of surface points. It will be described later that traceability of the measurement cannot be however assured due to the lack of standards. At the moment, first drafts of standards are available. However, several ways how to achieve traceability exists. This is realized by applying methods valid for tactile measuring machines, such as CMMs. Advantages, disadvantages and suggestions and solutions for achieving traceability in CT are summarized below.

**Advantages**

- Non-destructive
- Determination of inner and outer geometry
- Volume of data of high density
- Short scanning time

**Disadvantages**

- No accepted test procedures available so far
- Complex and numerous influence quantities affecting measurements
- Reduced form measurement capability due to measurement errors (artefacts)
- Measurement uncertainty in many cases unknown (results are not traceable)
- Problem encountered when scanning multiple materials within one product

**Suggestions and solutions**

- Apply calibrated standards to correct measurement errors and achieve traceability
- Perform tests to understand the influence of error sources
- Evaluate task specific measuring uncertainty
- Adopt experience from coordinate metrology to CT [30]

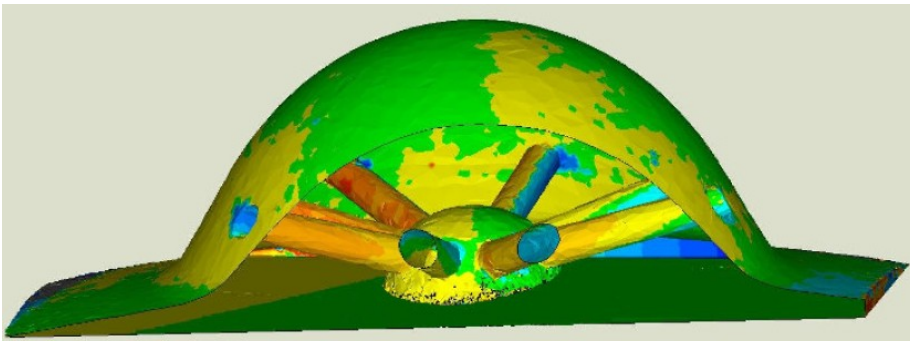

Figure 3.11: *Actual/Nominal comparison between a CT scan and a CAD model on a diesel injector [23].*


Figure 3.12: *Reverse engineering; 1: Manufacturing according to the CAD drawings; 2: 3D digitizing through CT; 3: 3D comparison with original CAD; 4: RE: modification of CAD or manufacturing process [Source: Rx solutions].*

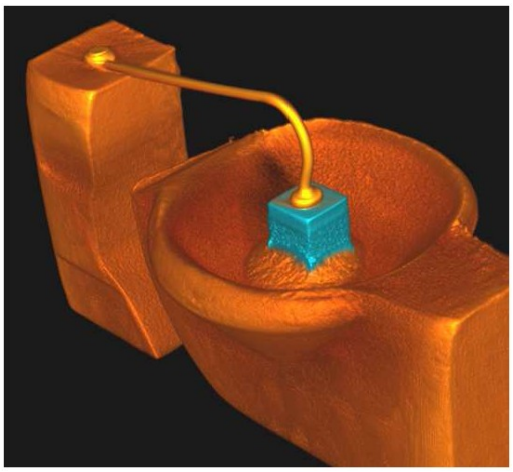

Figure 3.13: *Light Emitting Diode (LED). High resolution of 3D data enables to distinct different materials: Cu, Au and Si [25].*

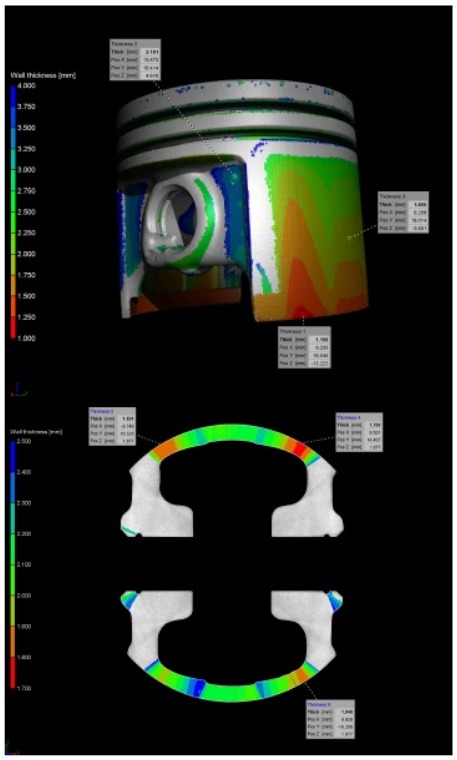

Figure 3.14: *Wall thickness analysis on aluminum casting [31].*

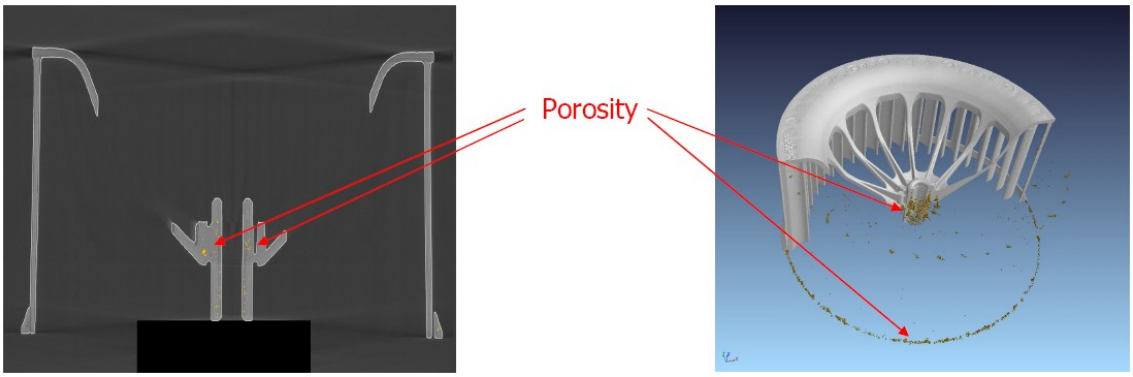


Figure 3.15: *Porosity inspection on a car inlet fan [23].*

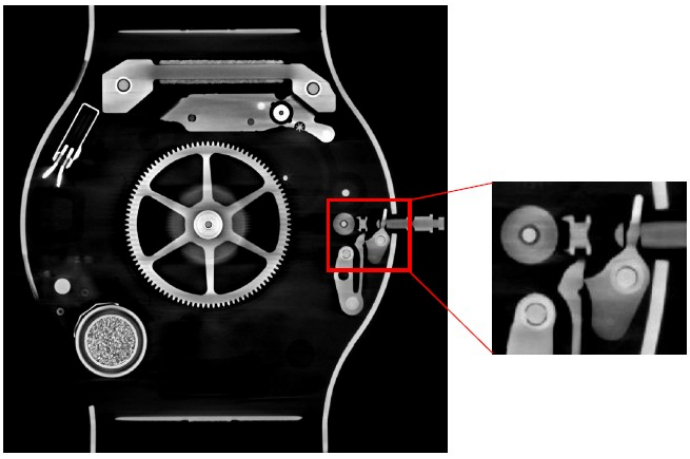

Figure 3.16: *Assembly inspection to monitor correct mechanism/functionality of watches [23].*

# Chapter 4

# Influence factors

There are numbers of influence factors in CT that play an important role in CT qualification. A visual overview of the most relevant influence factors in CT is shown in Figure 4.1. This chapter describes some of the most important influence parameters, their effect on CT quality and presents some techniques for compensating and/or reducing their effect on CT outputs proposed by different authors. The full overview of all the influence factors is presented in the German guideline VDI/VDE 2630 part 1.2 - Factors influencing the measurement results and recommendations for dimensional measurements in computed tomography [18].

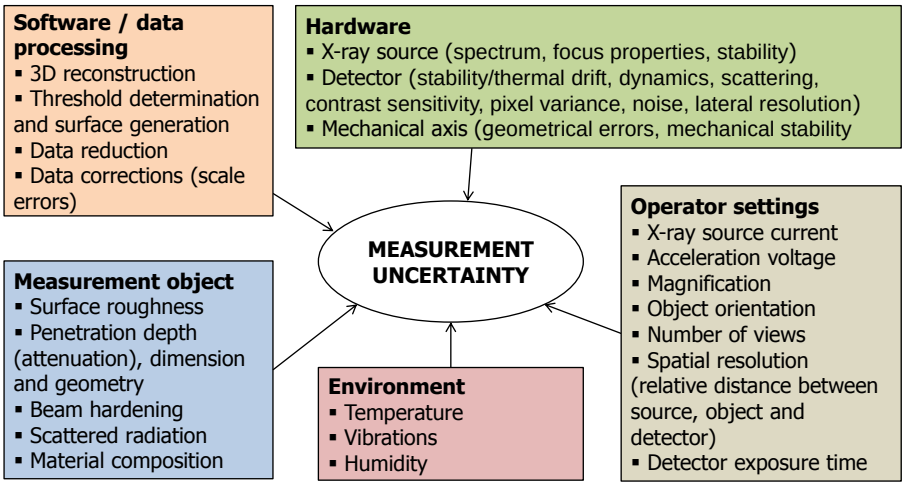


Figure 4.1: *Influence factors in CT.*

## 4.1 Hardware

### 4.1.1 X-ray source

#### State of the art and theoretical analysis

X-rays are electromagnetic waves with a wavelength smaller than about 10 nm. A smaller wavelength corresponds to a higher energy according to Equation 4.1. The energy of each photon, *E*, is proportional to its frequency, *f*, and is described as follows:

$$E = hf = \frac{hc}{\lambda} \tag{4.1}$$

where $h$ is Plank's constant ($h = 6.63 \times 10^{-34} Js$), $c$ is a speed of light ($c = 3 \times 10^{8} ms^{-1}$), and $\lambda$ is a wavelength of the X-ray. Therefore, X-ray photons with longer wavelengths have lower energies than the photons with shorter wavelengths. The X-ray energy is usually expressed in eV ($1eV = 1.602 \times 10^{-19} J$).

X-rays are produced when an accelerated beam of electrons is retarded by a metal object (target material, usually corresponding to the anode), with emission of X-ray photons. An X-ray source, shown in Figure 4.2, consists of a hot cathode (tungsten filament) and an anode inside a vacuum tube, between which an electrical potential is applied. Electrons ejected from cathode surface are accelerated towards the anode. When these electrons impinge on the target, they interact with these atoms and transfer their kinetic energy to the anode. These interactions occur within a very small penetration depth into the target. As they occur, the electrons slow down and finally come nearly to rest, at which time they can be conducted through the anode and out into the associated electronic circuit. The electron interacts with either the orbital electrons or the nuclei of the metal atoms. The interactions result in a conversion of kinetic energy into thermal energy and electromagnetic energy in the form of X-rays [32]. Since more than 98% of energy is turned into heat, the anode has to be water cooled [33]. The emitted X-rays consist of two components: (1) The first is called Brehmsstrahlung radiation and is the one described above and originates a continuos spectrum. (2) The second type of radiation is related to the excess of energy of the accelerated electron collades against an atom with the expulsion of an electron from the interior electronic orbits of the target atom. Excess of energy is emitted as a photon of X-ray with constant peak values of the wavelength (often referred to as characteristic K$\alpha$ radiation or peak X-ray energy). Since these spectrum peaks are different from material to material, this kind of radiation is called Characteristic radiation. An example of emitted spectrum for rhodium target is shown in Figure 4.3.

There are three types of radiation sources used in industrial CT scanners:

1. X-ray tubes
2. LINear ACcelerators (LINAC)
3. Isotopes

The first two are (polychromatic or bremsstrahlung) electrical sources; the third is approximately monoenergetic radioactive source. One of the primary advantages of

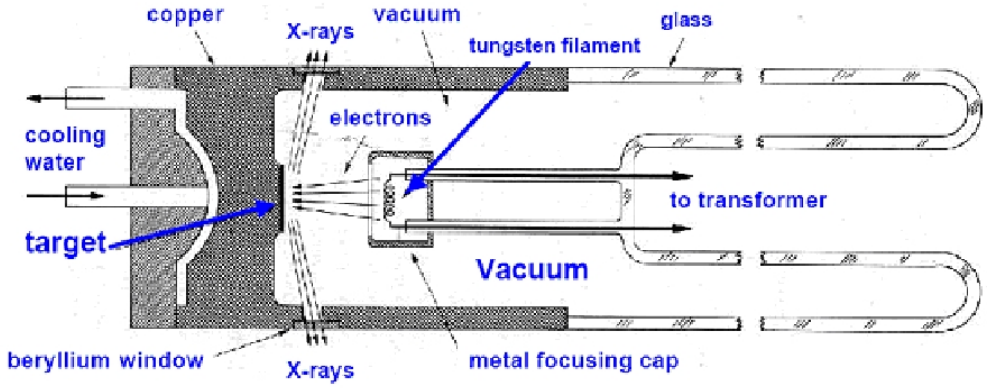


Figure 4.2: *Schematic overview of an X-ray source and its components [33].*

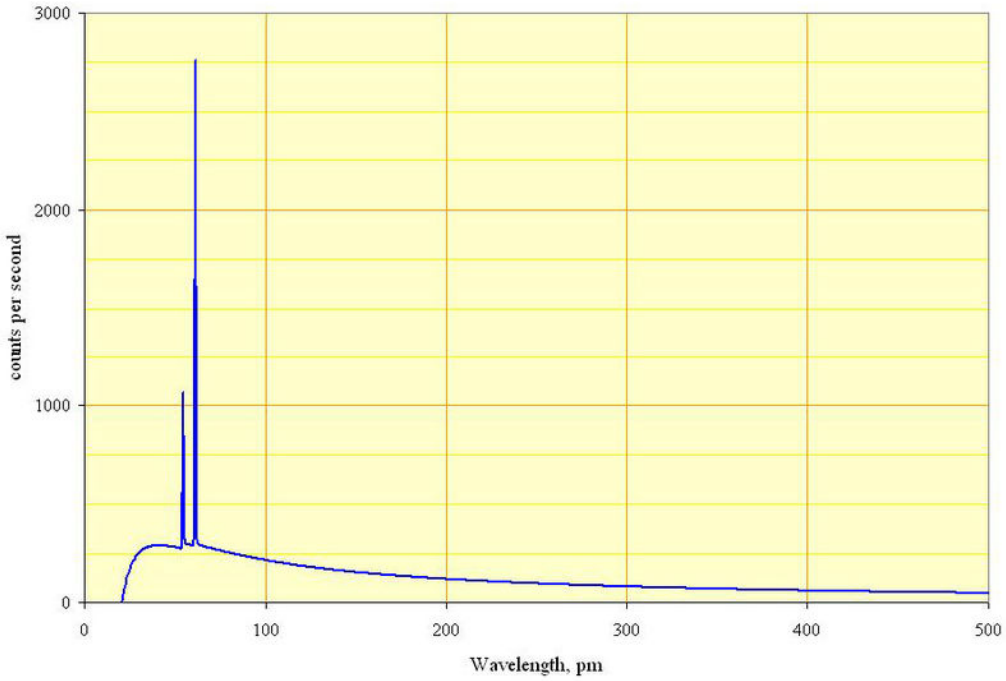


Figure 4.3: *Spectrum of the X-rays emitted by an X-ray tube with a rhodium target, operated at 60kV. The smooth, continuous curve is due to Bremsstrahlung radiation, and the spikes are characteristic K lines for rhodium atoms [Source: Wikipedia].*

using an electrical X-ray source over a radioisotope source is higher photon flux possible with electrical radiation generators, which allows shorter scanning times. The greatest disadvantage of using an X-ray source is the beam hardening effect associated with polychromatic fluxes (see Section 4.3.2 on beam hardening effect). Typical medical and industrial CT scanners employ X-ray tubes as X-ray source, but operate at different potentials (higher for industrial CT scanners). LINACs are used to scan very huge parts, which require high energy radiations, such as large rocket motors. Isotope sources offer the important advantage over X-ray sources because they do not suffer from beam hardening problems since isotopes are monoenergetic sources. Other advantages of

Table 4.1: Characteristics of common anode materials [34].

| Material | Advantages/Disadvantages |
|---|---|
| Cr | High resolution for large d-spacings, particularly organics/High attenuation in air |
| Fe | Most useful for Fe-rich materials where Fe fluorescence is a problem/Strongly fluoresces Cr in specimens |
| Cu | Best overall for most inorganic materials/Fluoresces Fe and Co K$\alpha$ and these elements in specimens can be problematic |
| Mo | Short wavelength good for small unit cells, particularly metal alloys/Poor resolution of large d-spacings; optimal kV exceeds capabilities of most HV power supplies |

using monoenergetic sources are that they do not require bulky and energy-consuming power supplies, and they have an inherently more stable output intensity. On the other hand, higher signal-to-noise ratio (SNR) affects source spot size and therefore limits resolution. For these reasons industrial applications of isotopic scanners are limited to applications which do not require high scanning time and resolution is not a critical parameter [35, 36].

The most important variables which determine the quality of X-ray emission spectrum are:

1. Focal spot size
2. Spectrum of generated X-ray energies
3. X-ray intensity

The focal spot size affects spatial resolution of a CT system by determining the number of possible source-detector paths that can intersect a given point in the object being scanned: blurring of features increases as the number of these source-detector paths increase [37]. Figure 4.4 illustrates the effect caused by the spot size. The smaller the spot size, the sharper the edges will be. In case of large spot sizes, blurring will occur, known as penumbra effect. Blurring effect is also connected with the geometrical magnification and will be discussed later in Section 4.5.1. A disadvantage of a smaller spot size is the concentrated heat produced at the spot on the target inside the X-ray tube, requiring cooled targets and limiting the maximum applicable voltage [38]. The target material (together with the previously mentioned characteristic radiation) determines the X-ray spectrum generated. The energy spectrum defines the penetrative ability of the X-rays, as well as their expected relative attenuation as they pass through materials of different densities. X-rays with higher energy penetrate more effectively than lower energy ones. Figure 4.6 shows dependency of the X-ray emission spectrum on the chosen target material. High atomic number elements like gold (Z=79) and tungsten (Z=74) enable to reach higher penetration (because the spectrum is shifted towards high energy levels), enhancing the efficiency of X-ray generation [37, 39]. The X-ray intensity is fundamentally limited by the maximum possible heat dissipation of the X-ray target. Exceeding a critical material dependent power density will result in evaporating the

target. Therefore, higher intensity requires larger target area and therefore limits the resolution of the measurement [16]. The X-ray tube current and voltage are variables that can be chosen by the operator within a machine specific range. While the current affects only the intensity (amount of radiation), without modifying the quality (penetration) of emission spectrum, tube voltage has an influence on both. Figure 4.5 shows that a change of tube current causes a change in the amplitude of X-ray spectrum at all energy levels but the curve shape is preserved. On the other hand an increase of tube voltage causes both an increase in amplitude and a shift of the curve towards high energy levels [37].

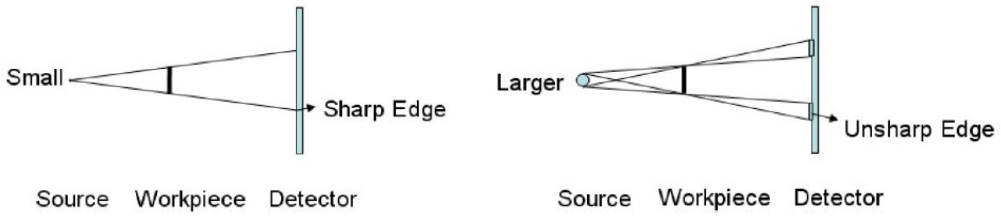


(a) *Small spot size.* (b) *Large spot size.*

Figure 4.4: *Influence of the spot size on the sharpness of the edge [38].*

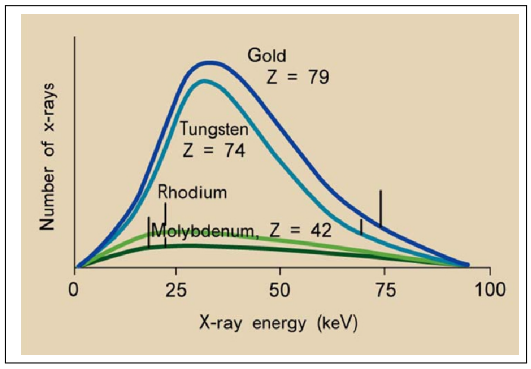


Figure 4.5: *Influence of the target material on the X-ray emission spectrum [39].*

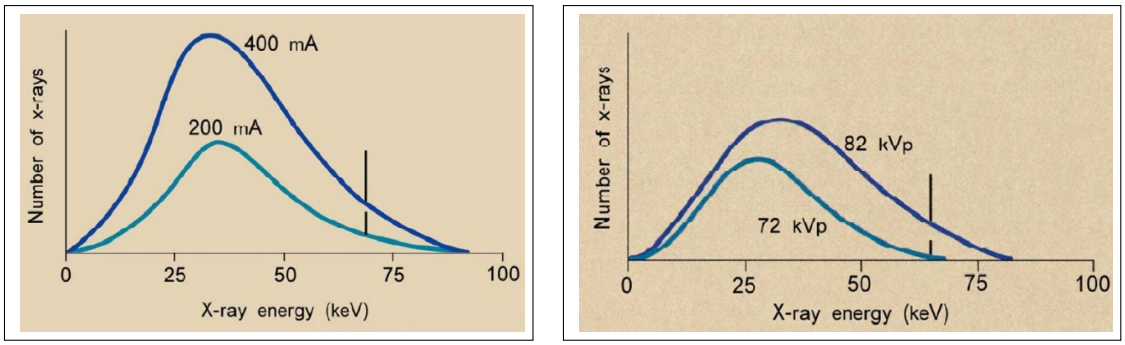


(a) *Current.* (b) *Voltage.*

Figure 4.6: *Influence of the tube current/voltage on the X-ray emission spectrum [39].*

**Experimental investigation**

One of the first approaches to reduce the effects of the beam hardening was the use of pre-filters. These filters, made of different materials like aluminum, copper or brass, are used to harden the X-ray spectrum generated by the X-ray tube. In this way, the spectrum approximates a monochromatic energy distribution because low energy photons are filtered out. The emission spectrum is not modified but it increases the average energy, with an increase of quality and a reduction of quantity (in terms of total energy). Figure 4.7 shows the emission spectrum of a 420 kV X-ray source with a tungsten target, filtered with a 3 mm aluminum and in addition with a 5 cm quartz. In the first case average energy is 114 keV. In the second case the energy average is shifted to 178 keV because of attenuation of low-energy radiation [40].

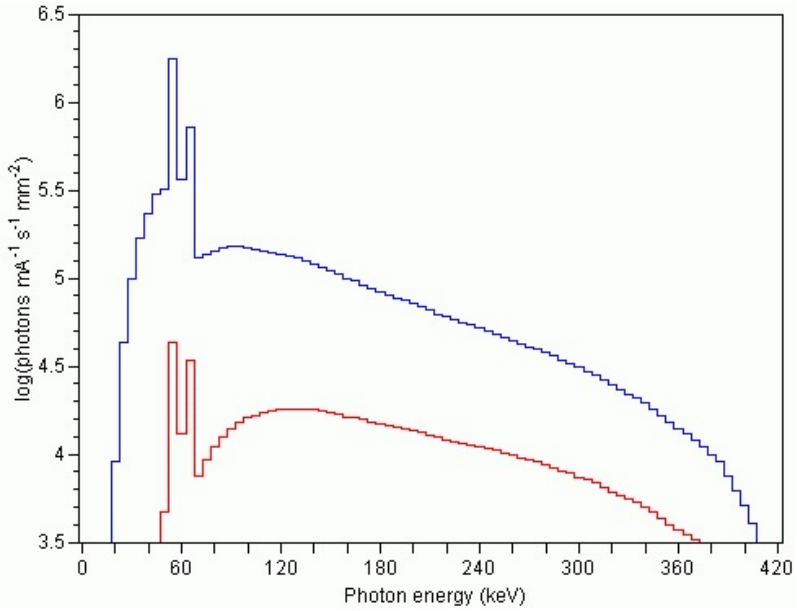


Figure 4.7: *X-ray emission spectrum for a 420 kV X-ray source with a tungsten target and filtered with 3 mm aluminium (upper blue curve) and also been passed through a 5 cm quartz (lower red curve) [40].*

A study concerning a CT device with two X-ray sources is presented in [41]. The two X-ray sources, 450 kV macro focus X-ray source and 250 kV micro focus, are used for advanced application, requiring characterization of a part, made of two or more materials. These investigations show that using the micro focus it is possible to obtain higher level of detail (thanks a lower spot size ranging between $5-200\ \mu m$). The problem is that there are more artefacts, particularly evident when two or more materials are present in the inspected part. The 450 kV source originates less artefacts but gives lower resolution (because of a spot size of 2.2 mm). This solution is therefore more indicative if a high level of details is not requested. Figure 4.8 shows a cross section of in industrial plug scanned using the two X-ray tubes. Results related to the micro-focus source show severe artefacts, surrounding the metallic pins, due to the presence of two materials with different attenuation coefficients. These artefacts are not present if the macro X-ray tube is used, even if same details of the housing are not visible [41].

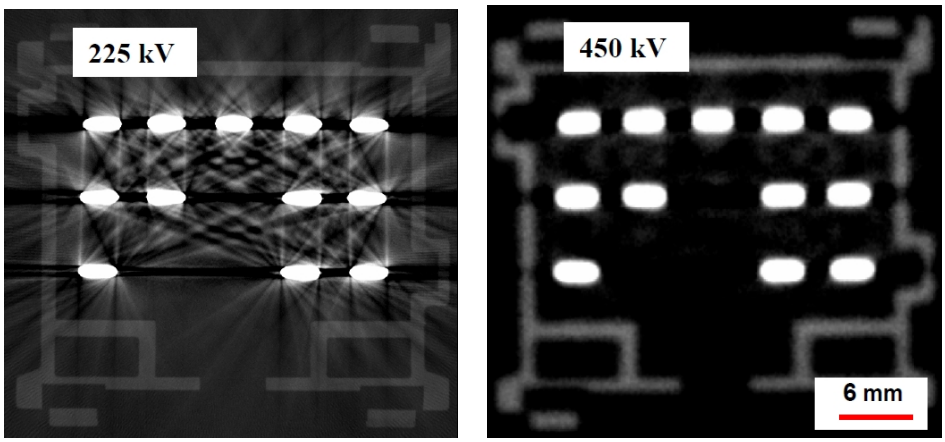


(a) *225 kV tube (tube voltage used 200 kV)* (b) *450 kV (tube voltage used 300 kV)*

Figure 4.8: *CT-cross sectional pictures of a commercial plug consisting of metallic pins and a polymeric housing [41].*

### 4.1.2 Rotary table

**State of the art and theoretical analysis**

When scanning, the part is mounted on the rotary table. System axis misalignment can introduce artefacts in the scanned data. The ideal system geometry is shown in Figure 4.9: The central ray intersect the center of the detector (point O); the rotation axis is perpendicular to the mid-plane and the mid-plane cuts the detector in the central row. Because of misalignments of the detector, X-ray source and/or rotary table, different artefacts can appear on the CT images, reflecting in artefacts in the reconstructed 3D geometry. Some examples of typical misalignment configurations are shown in Figure 4.10, Figure 4.12, Figure 4.13 and Figure 4.14. Figure 4.10 shows artefacts in the image arising when the detector shifts along the horizontal transverse direction (X axis). Figure 4.12, Figure 4.13 and Figure 4.14 show examples of artefacts caused by a tilt of the detector around its central row (X axis), a twist of the detector around its central column (Y axis) and a skew of the detector around the central ray. When the detector twists around its central column, there are no artefacts in the reconstructed images but the images have smaller resolution. The worst situation occurs when the detector skews around the central ray (see Figure 4.14(b)), because the effective width and height of the detector used in the reconstruction algorithm becomes smaller, which makes the reconstructed images flattened. This phenomenon leads to the most serious distortions in a CT image [42]. These outcomes are also confirmed in [43].

**Experimental investigation**

An experiment to quantify the maximum tolerable detector skew around the central axis using a ball bar and a monochromatic X-ray source in reported in [43]. Skews of the detector 0, 1/2, 1/4, 1/8 and 1/16 were applied. Results, in terms of maximum absolute differences between the reference volume and the volume after rotation, are shown in Figure 4.15. By applying a skew to the detector till 1/4 pixels will not affect dimensional

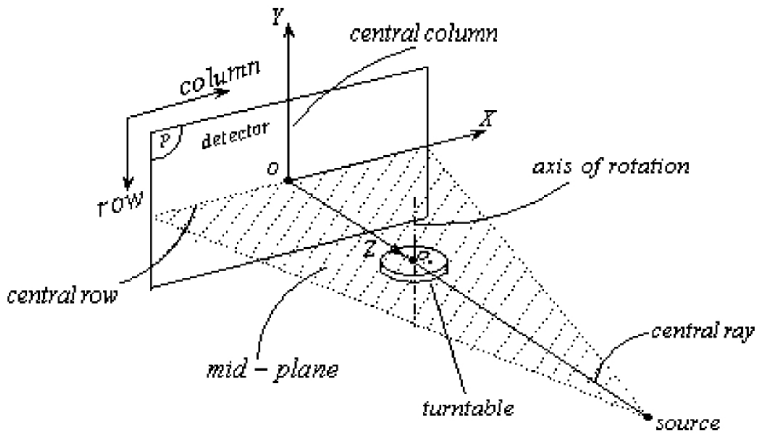


Figure 4.9: *Ideal geometry configuration for a cone-beam industrial CT scanner*

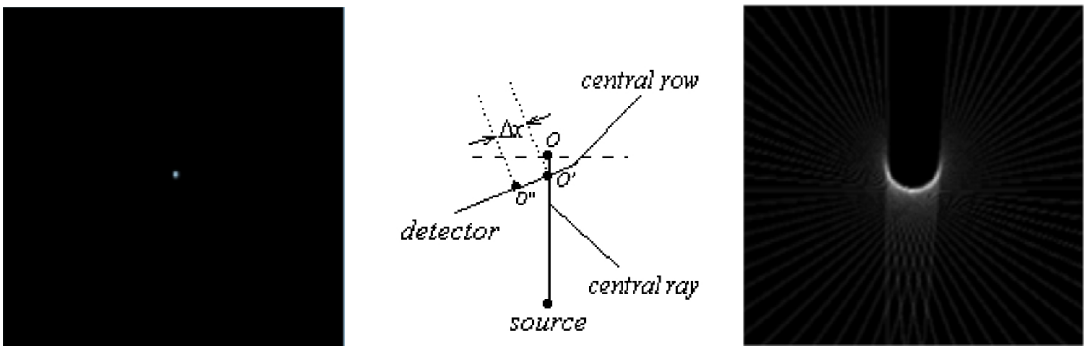


(a) *CT image of a dot without misalignment.*

(b) *Deviation of the detector from the ideal position.*

(c) *CT image of a dot with a misalignment of 10 pixel.*

Figure 4.10: *Misalignment effect due to horizontal transversal off-center shift along the detector column direction [42].*

Figure 4.11: *CT image without misalignment [42].*

measurements since the error will be of the order of magnitude of noise and artefacts of reconstruction [43].

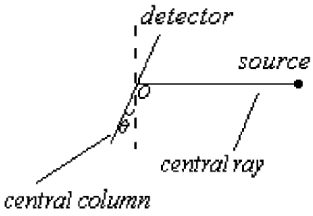


(a) *Deviation of the detector from the ideal position.*

(b) *CT image with a misalignment with a tilt around X axis of the detector.*

Figure 4.12: *Misalignment effect due to tilt of $\pi/10$ around detector central row [42].*

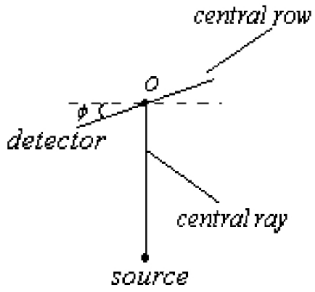


(a) *Deviation of the detector from the ideal position.*

(b) *CT image with a twist around Y axis of the detector.*

Figure 4.13: *Misalignment effect due to twist of $\pi/4$ around detector central column [42].*

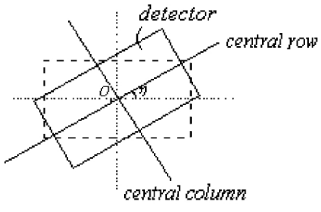


(a) *Deviation of the detector from the ideal position.*

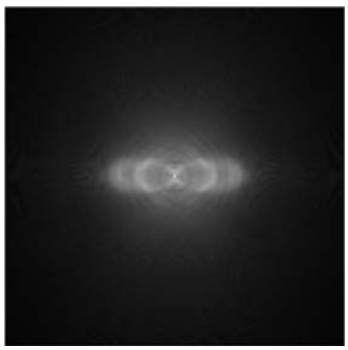

(b) *CT image with a skew around the central axis.*

Figure 4.14: *Misalignment effect due to skew of $\pi/7$ around the central axis [42].*

It is possible to compute CT system misalignment parameters through a calibration of the system. A method for calibration of the cone-beam CT system is reported in [42].

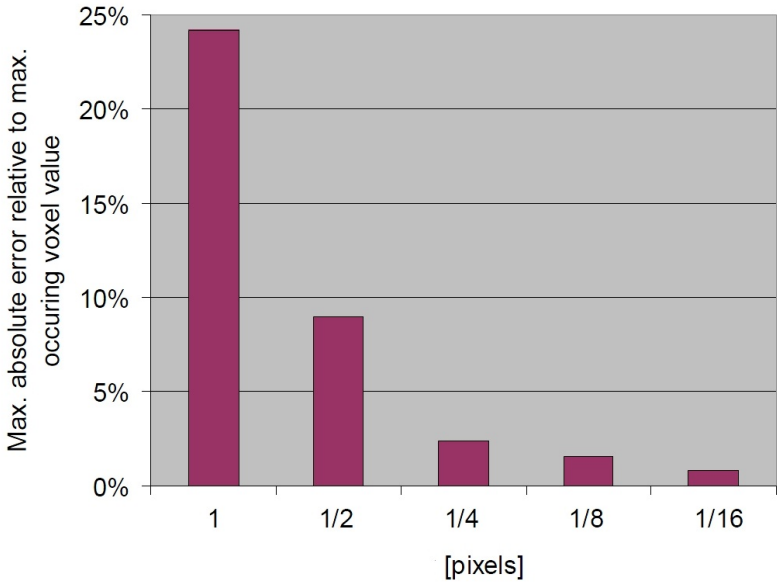


Figure 4.15: *Maximum tolerable detector skew around X-axis [43].*

Through this method it is possible to estimate analytically all misalignment parameters by using a four-point phantom and with just one angle projection. The calibration phantom is composed of a plastic cuboid with four small slices of high-density material attached to its surface. By knowing calibration lengths of the four sides of the square and the lengths of the four sides on the detector it is possible to estimate all parameters mathematically. The uncertainty of the method depends on the accuracy with which the center coordinates of the four calibration points are reconstructed.

### 4.1.3 X-ray detector

**State of the art and theoretical analysis**

An X-ray detector is used to measure the transmission of the X-rays through the object along the different ray paths. The purpose of the detector is to convert the incident X-ray flux into an electrical signal, which can then be handled by conventional electronic processing techniques. There are essentially two general types of detectors: (1) gas ionization detectors and (2) scintillation counters detectors. In the gas ionization detectors, the incoming X-rays ionize a noble element that may be in either a gaseous or, if the pressure is great enough, liquid state. The ionized electrons are accelerated by an applied potential to an anode, where they produce a charge proportional to the incident signal. A single detector enclosure can be segmented to create linear arrays with many hundreds of discrete sensors. Such detectors have been used successfully with 2MV X-ray sources and should be used with higher energies. Scintillator counter detectors exploit the fact that certain materials has the useful property of emitting visible radiation when exposed to X-rays. Sensors suitable for CT can be engineered by selecting fluorescent materials that scintillate in proportion to the incident flux and coupling them to some type of device that converts optical input to an electrical signal. The light-to-electrical

conversion can be accomplished in many ways. Methods include use of photodiodes, photo multiplier tubes or phosphor screens coupled to image capture devices (i.e. Charged Couple Displays (CCDs), video systems, etc.). Most recently, there are area detectors (panels) that provide a direct capture technique, utilizing amorphous silicon or amorphous selenium photo-conductors with a phosphor coating, which directly convert incident radiation into electrical charge. Like ionization detectors, scintillation detectors afford considerable design flexibility and are quite robust. Scintillation detectors are often used when very high stopping power, very fast pulse counting, or areal sensors are needed. Recently, for high resolution CT applications, scintillation detectors with discrete sensors are reported with array spacings in the order of $25\ \mu m$. Both ionization and scintillation detectors require considerable technical expertise to achieve performance levels acceptable for CT [36].

Important parameters of X-ray detectors are: quantum efficiency, number of pixels, read out speed (frame rate) and dynamic range. Quantum Efficiency (QE), or better Detective Quantum Efficiency (DQE), is described as the ratio between the squared output SNR to the squared input SNR. It describes the efficiency of transferring. The squared input SNR quantifies the number of photons and noise impinging the detector and the squared output SNR describes the output energy (incident photons and noise) from the detector. DQE affects the quality and intensity of signal of a given X-ray beam because describes the efficiency of transferring the energy of the input SNR of the incident X-ray beam out of the detector [36]. X-ray detectors have QE ranging from 2 to 50%, which strongly depends on the energy of the radiation and decreases with increasing energy. The QE can be increased by making the detector thicker or using materials which have higher values for the coefficient of absorption $\mu$ [44]. An important milestone in the development of detectors is the flat panel detector which guarantees geometrical precision of the pictures and efficient transport of the light from the scintillator to the photodiodes. A significant improvement in conversion is obtained with the direct conversion of the photons by semiconductors. The major advantage is the much higher photon sensitivity (single photon counter) and the capability of resolving photon energy. Currently applied semiconductor materials for sensors are CdTe, CdZnTe, Si and GaAs [45]. On the other hand, these are characterized by less quality in some other features, e.g. dynamic range, hot or dead pixels, and have smaller number of pixels and possible segment displacement. The improvement of flat panel detectors using scintillation technology was primarily based on increasing the number of pixels (up to the range of $10^7$pixels) and the size of the detector. The dynamic range is the range between the maximum and minimum radiation intensity that can be displayed. The maximum dynamic range of flat panel detectors is 16 bit. The frame rate of large area detectors is in the range of 2 to 9fps [16].

## 4.2 Software/data processing

### 4.2.1 3D reconstruction

**State of the art and theoretical analysis**

When the acquisition process of the scanned object is completed, reconstruction algorithms are used to reconstruct the 3D volume. These reconstructed 3D images are made of voxels. As can be seen from Figure 4.16, voxels are primitive elements of 3D structures. The size of the voxel is a function of the pixel size and the distance between the source-object and source-detector (this will be explained in details in Section 4.5.1 concerning the influence of magnification).

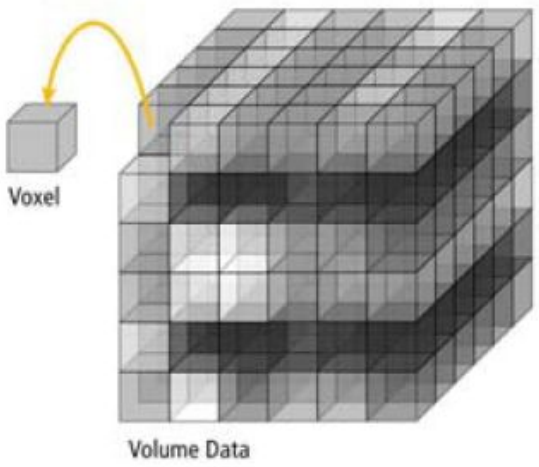


Figure 4.16: *Definition of a voxel [29].*

During the reconstruction, some errors can arise, such as systematic discrepancies between the values in the voxels and the attenuation coefficient of the object. This is mainly due to the beam hardening and movement of the part during acquisition.

### 4.2.2 Threshold determination and surface generation

**State of the art and theoretical analysis**

As is was described in Section 3.1, threshold value is a critical parameter in CT and is used for accurate image segmentation and surface data determination which influence the resulting reconstructed geometry of the scanned object [19]. Threshold converts a gray value image into a binary one. The resulting image then comprises of two sets: one represents the background (e.g. black), the other one the object (e.g. white). In principal, a threshold determines where are the boundaries between the object and the air, so that a surface can be assigned to the scanned object. The determination of the threshold takes place within each of the voxels the 3D model consists of, see a green line in Figure 4.17.

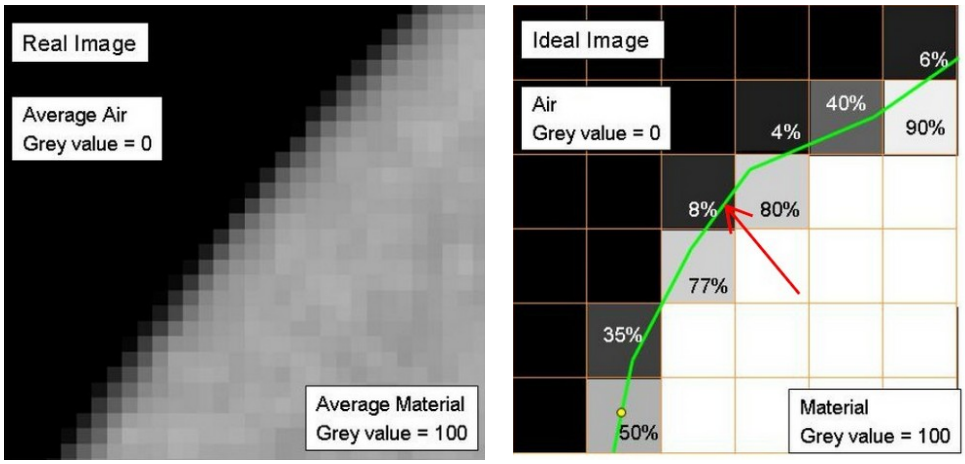


(a) *Real image.* (b) *Ideal image.*

Figure 4.17: *Application of threshold. The greed line represents an edge segmentation of the object/material from the air [46].*

A clear demonstration of how important is to select a proper threshold value can be seen in Figure 4.18. Here, a threshold is varied over a certain range and corresponding diameter of a cylindrical part is measured.

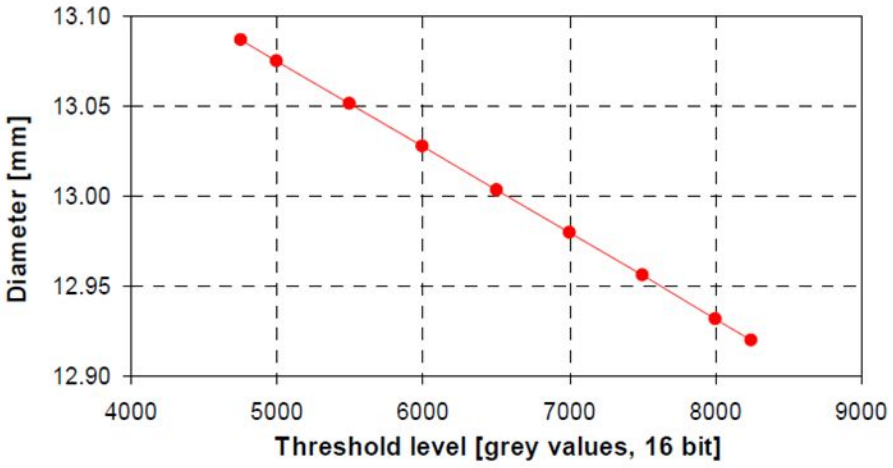


Figure 4.18: *Variation in diameter measurements of a cylindrical part for different threshold values. Diameter is calculated by Gaussian fitting of an ideal cylindrical surface to the resulting CT point cloud [19].*

Using specially designed reference objects, e.g. a hole bar [19], where the threshold value can be accurately evaluated by the simultaneous measurement of internal and external features. The dimensions of such features measured on CT data are strongly dependent on the exported threshold value. It is important to notice that dimensions of inner and outer features depend on changing threshold in the opposite way, see Figure 4.19. Once the CT measurements are performed and compared with the calibrated values (e.g. by

CMM), the correct threshold value is determined. This value is then used for a proper segmentation between the air and the material of the real component with the same or similar material properties as of the reference object. A study on the application of the threshold determination is discussed in [47].

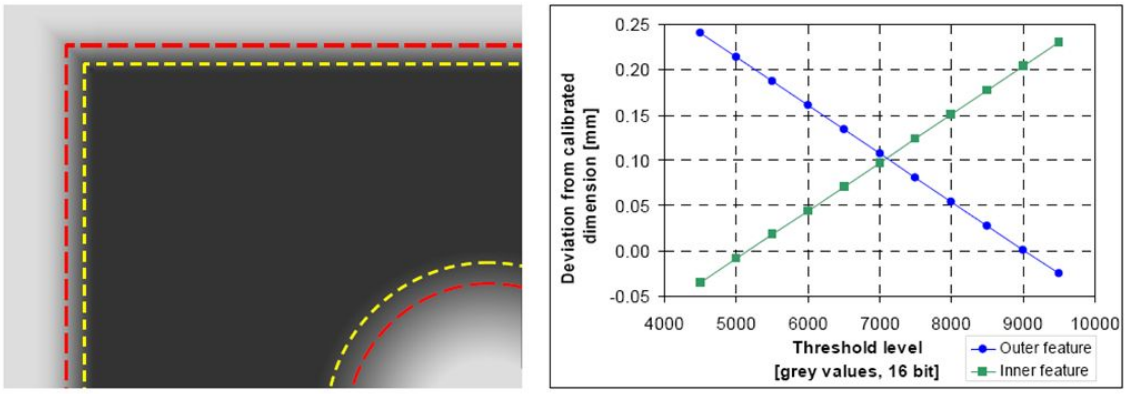


Figure 4.19: *Representation of the opposite behavior of changing thresholds on CT measurements for inner (circular hole) and outer (rectangular edge) features: Red and yellow lines represent the edges determined with two different thresholds (left); Deviations of measured dimensions with respect to calibrated values (right) [19].*

For example, a software **VGStudio MAX 2.0** for surface extraction, offers two threshold methods: advance and automatic. One of the advantages of the advance method against the automatic is higher precision of the threshold location. On the contrary, this method is slower and requires longer computation time. Figure 4.20 shows a threshold value determination for single (Figure 4.20(a)) and multiple (Figure 4.20(b)) materials. The peak on the left represents the background and the peak on the right represents the material. The red line then corresponds to the threshold value (so called ISO-surface) determined to segment the air and material.

#### Experimental investigation

An investigation different threshold methods was performed in [48], but since this investigation also concerns influence of the number of projections, it is presented in Section 4.5.3.

### 4.2.3 Data reduction

#### State of the art and theoretical analysis

In the late 80's, when CT has been introduced to the industrial word and used for non destructive testing in industrial applications, the size of the image, which was the 2D cross section of the sample, was in the range of 256x256 pixels. In 90's, when the sample could be imaged in full 3D appearance, the image size was increased to 512x512 pixels. In this period, quantitative measurements within the whole 3D reconstructed model could have been performed. The accuracy of the CT systems became better as well. When

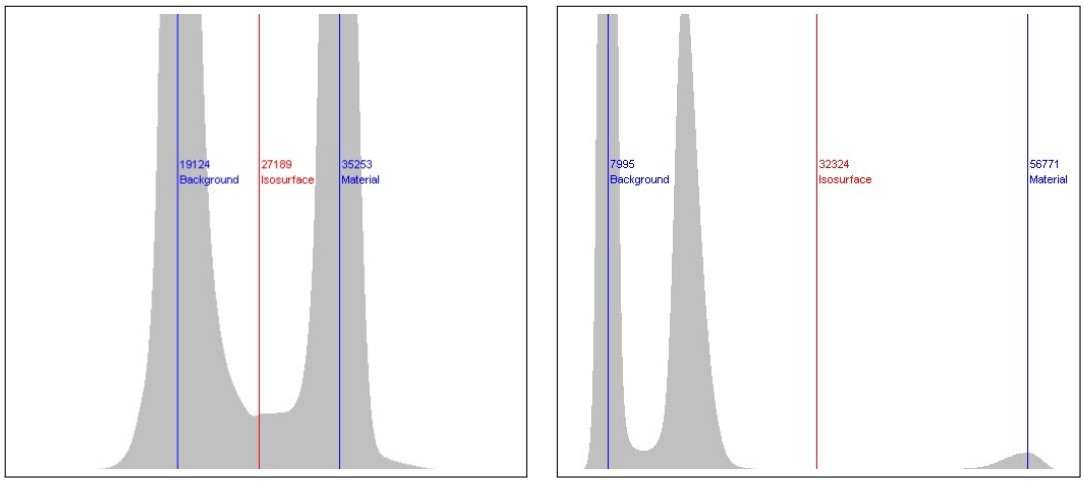


(a) *Single material.* (b) *Multiple material.*

Figure 4.20: *Threshold value determination in VGStudio MAX software.*

the time passed, the amount of data within a single data set became larger by scanning a larger number of images. When the flat detectors started to be used later on, the standard image size became 1024x1024 pixels. Today, a 1024x1024 pixel detector produces a 2 GByte data set within an hour or less. In some cases, a single data set can be produced in a size up to 8 GByte [2].

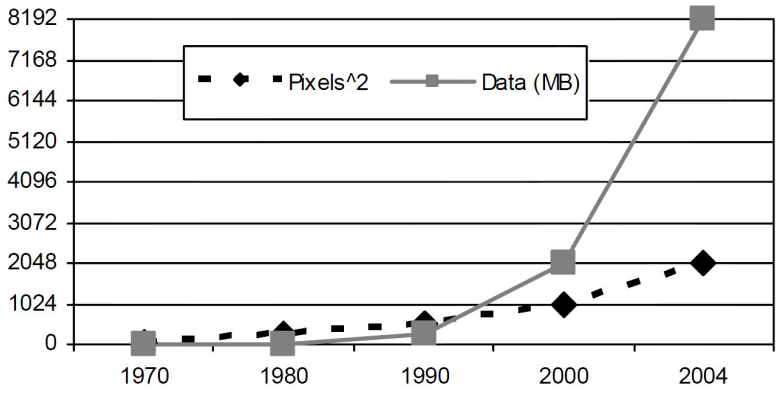


Figure 4.21: *Increase in CT image sizes and data set size.*

One of the main challenges today is to find a way to process a big amount of CT data going from the CT scanner to the reconstruction cluster and then to the computer's memory for visualization and later for complex 3D analysis in a relatively short time. Today, this task takes several minutes.

As it was mentioned in Section 3.5, one of the main advantages of CT is the fact that the reconstructed model consists of a high density of measuring points. Other measuring techniques like optical instruments and CMMs do not offer so high density measuring points. It was also mentioned in Section 3.1 that after the surface is defined by applying correct threshold value, the surface is extracted either as a point cloud or as an STL

file in the form of a polygonal mesh, visualized as triangles. The number of triangles has to be further optimized so that a software for visualization is able to handle this task. By decreasing the number of triangles, the original geometry is affected and leads to degradation of the quality of the CT scan. Another possibility how to perform measurements is to measure directly on the voxel based model, as is also presented in Figure 3.2. This however means to handle a big amount of data and requires high performance PC with high memory.

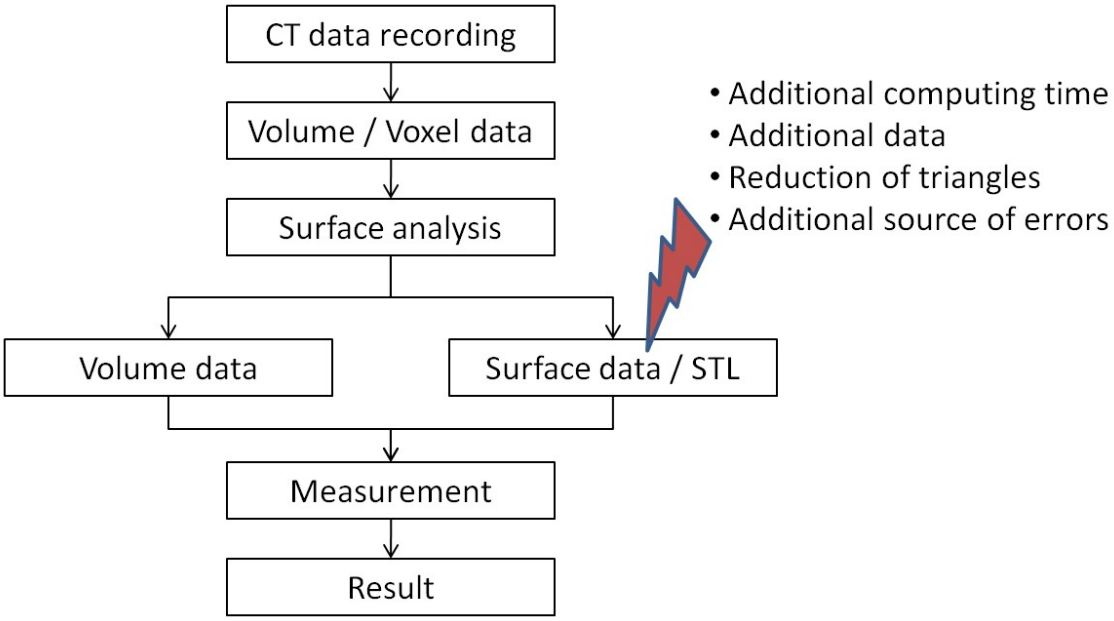


Figure 4.22: *Modified process chain for CT measurements.*

**Experimental investigation**

A comparison between voxel and STL data was done in [49]. A plastic component was scanned using two CT scanners and selected geometrical and dimensional tolerances were measured and evaluated on either voxel and STL data. Results show deviations up to 25 $\mu m$ for some parameters, assessing a significant modification of the original data due to the STL extraction.

The item under investigation was the housing (cylindrical part) of the FlexPen®(see Figure 4.23). The material of the FlexPen's housing was polypropylene (PP). Reference measurements were performed using CMM. The item was then scanned on two CT scanners. The scanning parameters are summarized in Table 4.2.

After the item was scanned using both CT scanners, a direct measurement on the voxel model was performed using softwares for 3D reconstruction dedicated to above mentioned CT scanners, or the surface was extracted on the reconstructed 3D model and saved as an STL file and the measurements were performed in another inspection software (GOM ATOS) for analysis of results. Two STL surface extraction methods were


(a) *Insulin FlexPen®.* (b) *Housing of the FlexPen®.*

Figure 4.23: *Item under investigation - FlexPen®.*

Table 4.2: Scanning parameters for two CT scanners.

| | Voltage kV | Current $\mu A$ | Voxel size $\mu m$ | No of proj. | Int. time ms |
|---|---|---|---|---|---|
| CT scanner M | 150 | 200 | 134 | 720 | 1000 |
| CT scanner N | 100 | 100 | 50 | 720 | 500 |

applied using one of the softwares: (1) Precise and (2) Precise with simplification. The difference between both mentioned STL extraction method is in different algorithms for creation of polygonal mesh.

Since the geometrical measurements can be affected by systematic errors, a scale factor correction technique was applied (more about scale factor correction in Section 4.2.4) to all measurements using a ball bar.

Detailed description of all investigated geometrical and dimensional tolerances is given in [49]. Here, the authors discuss only selected tolerances: parallelism, coaxiality, distance and diameter. Results are summarized in Figure 4.24. Four important comparative observations can be analyzed. These are:

1. Measurements on voxel and STL
2. Two STL extraction methods (precise vs. precise with simplification)
3. Performance of both CT scanners
4. Measurements on CMM and CT scanner

It can be seen from Figure 4.24 that measurements performed on the voxel data result in smaller deviations with respect to the calibrated values compared to measurements performed on STL. Experimental standard deviations are in all cases smaller for measurements on voxel data. Measurements performed on CT scanner N are for most

of the verified tolerances smaller than measurements on CT scanner M. The two STL extraction methods do not present any significant differences.

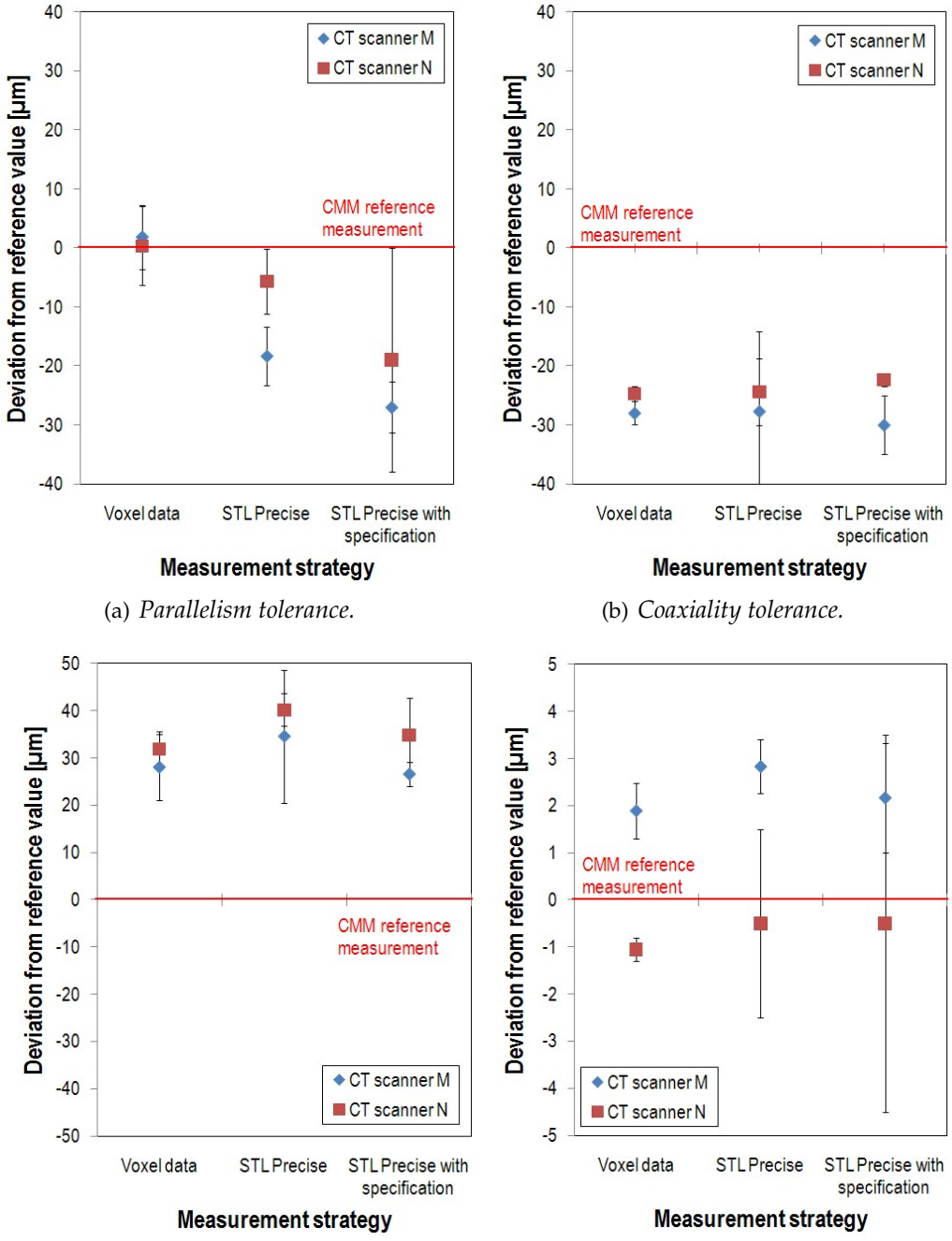


(a) *Parallelism tolerance.* (b) *Coaxiality tolerance.*

(c) *Distance tolerance.* (d) *Diameter tolerance.*

Figure 4.24: *Deviations of selected dimensional and geometrical tolerances with respect to calibrated values. Error bars represent experimental standard deviation based on three repeated measurements.*

### 4.2.4 Data correction (scale factor correction)

**State of the art and theoretical analysis**

Determination of scale factors in all space directions can be performed using reference objects, e.g. hole bars or ball bars (see Figure 4.25). This is concretely achieved through the evaluation of the distance between the balls centers (ball bar) or holes axes (hole bar), respectively. Simply, the distance measured with CT is compared to the calibrated distance. The use of these reference objects has specific advantages: the distance between the balls and holes respectively is very easily measurable on CT data points as the distance of two fitted spheres or cylinders respectively over the corresponding point cloud portions. Furthermore, the distance of sphere centers or holes axes respectively measured on CT systems is nearly independent from the threshold applied for the surface data extraction. This makes the evaluation of scaling factors very robust and independent from threshold determination [19].

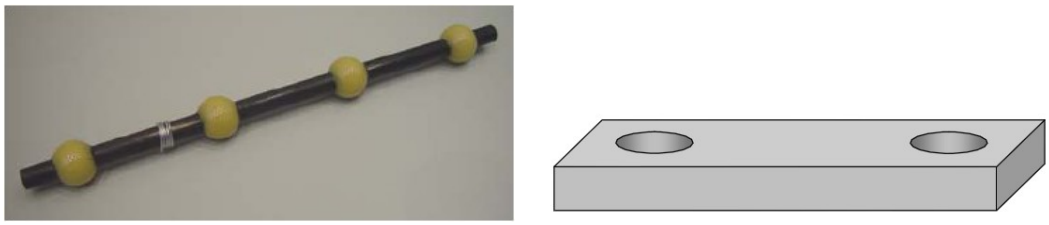

(a) *Ball bar [26].* (b) *Hole bar [19].*

Figure 4.25: *Examples of reference objects in CT for scale factor correction.*

The *CF* is based on recalculating of the original voxel size ($s_0$) using a reference object. The *CF* is calculated as expressed in Equation 4.2.

$$CF = \frac{\text{Reference value}}{\text{Measured value}} \tag{4.2}$$

After that, the new voxel size $s$ is calculated as follows:

$$s = s_0 \cdot CF \tag{4.3}$$

It was however mentioned in [50] that a common procedure for CT data correction applied for industrial CT systems is based on the correction of the nominal voxel size with the known diameter of the core hole of the micro gear (assessed by tactile micro CMM measurements), as the micro gear was the item under investigation.

It was investigated in [26] that scaling factors up to 1.01 were observed on different CT systems as relative length measurement errors, i.e. a sample of 100mm length is measured with a measurement deviation of up to 1mm. Another observation was achieved in [26] on an industrial 450 kV 2D-CT system. Scaling factors were found to change over a long period of time, see Figure 4.26. This was due to changes in the system geometry. It is therefore required to scan the reference object simultaneously together

with the sample under study and so to evaluate and correct for scaling errors.

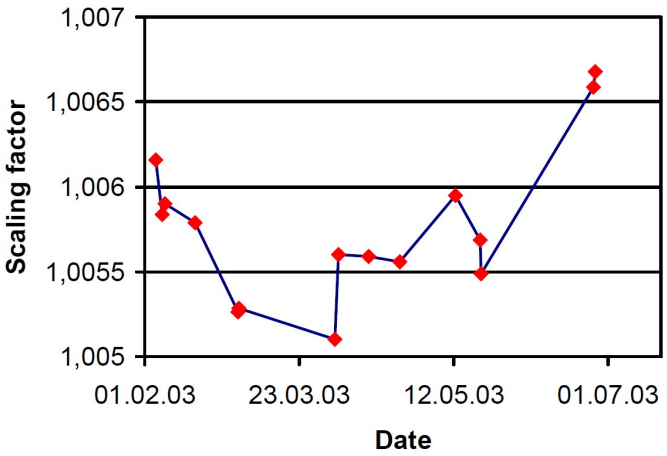


Figure 4.26: *Change of the scale factor in time [26].*

## 4.3 Measurement object

### 4.3.1 Penetration depth (attenuation), dimension and geometry

**State of the art and theoretical analysis**

Interaction of the X-rays (photons) with matter is of electromagnetic nature. In theory, an interaction can result in only one of three possible outcomes:

1. The incident X-ray can be completely absorbed and cease to exist
2. The incident X-ray can scatter elastically
3. The incident X-ray can scatter inelasitcally

The interaction between the photons and the matter can happen in only four ways:

1. They can interact with atomic electrons
2. They can interact with nucleons (bound nuclear particles)
3. They can interact with electric fields associated with atomic electrons and/or atomic nuclei
4. They can interact with meson fields surrounding nuclei

Thus, in principle, there are twelve distinct ways in which photons can interact with matter, see Table 4.3.

**Photon absorption** is an interaction process when the photons disappear and all their energy is transferred to atoms of the material. **Photon scattering** is an interaction process

Table 4.3: X-ray interactions with matter [24].

| Matter | Effects of interaction | | |
|---|---|---|---|
| | Complete absorption | Elastic scattering | Inelastic scattering |
| Atomic electrons | Photoelectric effect | Rayleigh scattering | Compton scattering |
| Nucleons | Photo disintegration | Thomson scattering | Nuclear resonance scattering |
| Electric field of atom | Pair production | Delbruck scattering | Not observed |
| Meson field of nucleus | Meson production | Not observed | Not observed |

when the photons do not disappear, but changes direction of their propagation. In addition, the scattered photons may transfer a part of their energy to atoms or electrons of the material.

The primary important interactions between the X-rays and the matter to X-ray imaging are shown in Figure 4.27. These are:

- Photoelectric effect
- Compton scattering
- Pair production

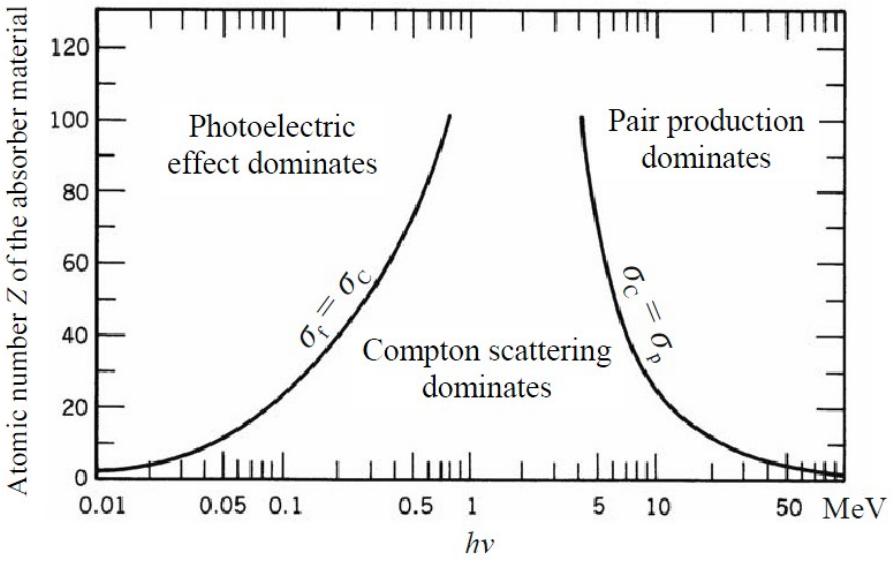


Figure 4.27: *The three principal interaction regions of X-rays with matter are plotted as a function of the atomic number versus the radiation energy.*

The three principal X-ray interaction mechanisms are schematically illustrated in Figure 4.28.

- **Photoelectric effect**: This effect causes an incident X-ray to interact with an electron within an inner-shell. Hereby the electron will be ejected from the atom (see Figure 4.28(a)). If the photon carries more energy than is necessary to eject the electron, it will transfer this residual energy to the ejected electron in the form of kinetic energy. The X-ray photon is thus completely absorbed. The photoelectric effect is predominant at low X-ray energies and depends strongly on the atomic number [32].

- **Compton scattering**: This process, also known as incoherent scattering, occurs when the incident X-ray photon interacts with an outer electron. The photon scatters inelastically, which means that the X-ray loses energy in the process. To conserve energy and momentum, the electron recoils and the X-ray is scattered in a different direction at a lower energy (see Figure 4.28(b)). Although the X-ray is not absorbed, it is removed from the incident beam as a consequence of having been diverted from its initial direction. Compton scattering predominates at intermediate energies and varies directly with atomic number per unit mass [32].

- **Pair production**: The incident X-ray interacts with the strong electric field surrounding the nucleus and ceases to exist, creating in the process an electron-positron pair. Pair production predominates at energies exceeding 1.022MeV (see Figure 4.28(c)) [32].

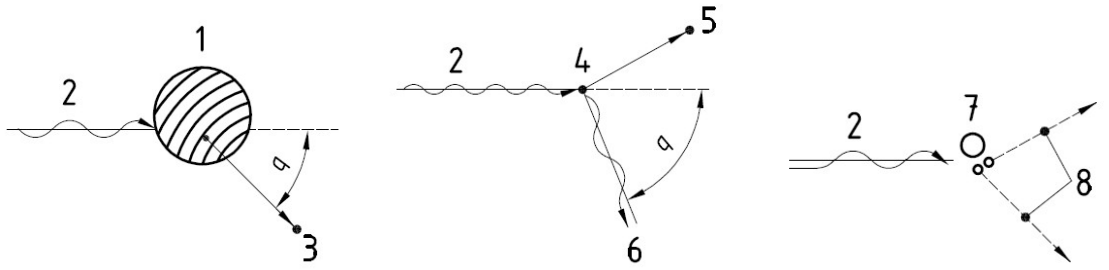


(a) *Photoelectric effect.* (b) *Compton scattering.* (c) *Pair production.*

Figure 4.28: *X-ray interaction mechanisms. 1-Atom, 2-Incident photon, 3-Photoelectron, 4-Atomic electron, 5-Compton electron, 6-Compton scattered electron, 7-Atomic nucleus, 8-Electron pair [36].*

It was mentioned in Section 4.1.1 that a beam of X-rays is characterized by its photon flux density or intensity and spectral energy distribution. When a beam of X-rays passes through homogeneous material, the intensity of the rays is decreased due to scattering and absorption. For monochromatic radiation with an incident intensity, $I_0$, the X-ray beam is attenuated after passing through a sample of thickness, $s$; to yield an attenuated intensity, $I$, with a magnitude described by Lambert–Beer's law. $\mu$ in the following equation is the linear attenuation coefficient (units 1/length).

$$I = I_0 e^{-\mu s} \tag{4.4}$$

If the X-rays are traveling through an inhomogeneous material, Equation 4.4 must be rewritten in more general form:

$$I = I_0 e^{-\int \mu ds} \tag{4.5}$$

Despite of the fact that X-ray sources emit polychromatic X-rays (except of Synchrotron radiation (more about Synchrotron radiation in Section 4.3.2)) consisting of a spectrum of different wavelengths, which are subject to preferential absorption of the lower energy photons, application of the X-ray technique generally assumes that attenuation is governed by Equation 4.4. As will be discussed later, the preferential adsorption of low energy photons of the polychromatic beam causes artefacts [22].

A line integral is taken along the direction of propagation and $\mu(s)$ is the linear attenuation coefficient at each point on the ray path. The linear attenuation coefficient is a measure for the attenuation per unit distance. It is specific for the used X-ray energy and for the type of absorber. Consequently, Equation 4.5 has to be adapted for inhomogeneous materials and polychromatic X-rays and can be expressed as follows:

$$I = \int I_0(E) e^{-\int \mu(s,E) ds} \, dE \tag{4.6}$$

When the CT technique was developed by Housfield in 1973 to determine the spatial distribution of attenuation values within the object from multiple ray measurements, CT required the development of mathematical reconstruction techniques capable of inversely solving a modified version of Equation 4.4, allowing for the estimation of the spatial variation of attenuation values along the ray path:

$$I = I_0 e^{-\int_s \mu(x) dx} \tag{4.7}$$

In this equation, the attenuation of each individual voxel is determined by the phase composition within each voxel.

A value of linear attenuation coefficient accounts generally for the number of atoms in a cubic cm volume of material and the probability of a photon being scattered or absorbed from the nucleus or an electron of one of these atoms. The number of photons transmitted through a material, corresponding to the linear attenuation coefficient, depends on the thickness, density and atomic number of the material and the energy of the individual photons, and generally reduces exponentially while traveling through the matter which can be seen in Figure 4.29. A schematic picture of the influence of atomic number and density of material on transmitted intensity in the form of X-ray photons is shown in Figure 4.30. The large circles In Figure 4.30(a) and Figure 4.30(b) represent individual atoms of high atomic number and small circles represent atoms of low atomic number. Atoms of high atomic number present higher probability of interaction with the photons rather than atoms of low atomic number. The attenuation should be higher for 'big atoms'. In other words, the X-rays have a greater probability of being transmitted (or penetrate deeper) through the matter for low atomic number. Figure 4.30(c) and Figure 4.30(d) show that smaller amount of atoms representing low density matter will give rise to less attenuation than a high density matter since the chances of interaction between the X-ray photons and the atoms are lower. Therefore, X-rays will penetrate

light materials better than heavy (dense) materials. Heavier, more dense materials offer greater resistance to X-rays penetration because they absorb more of the energy.

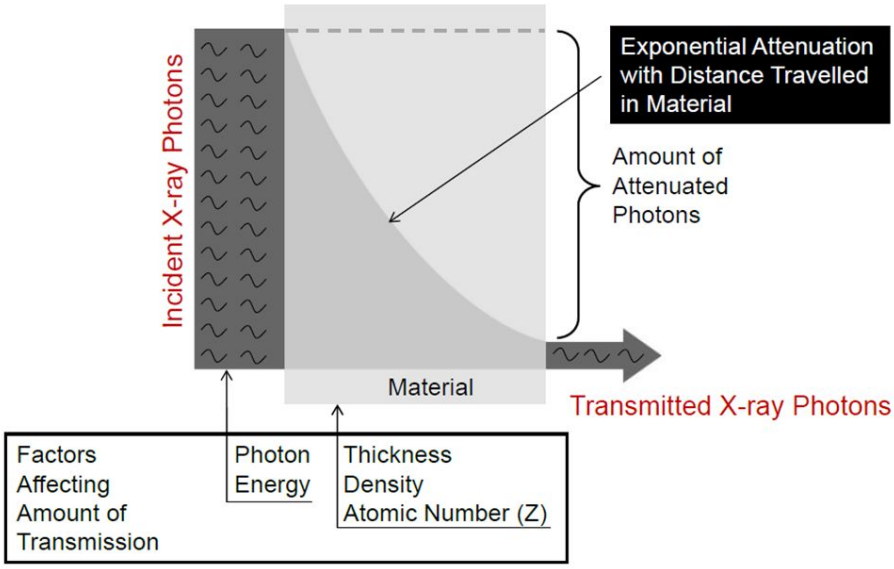


Figure 4.29: *Dependence between number of emitted and transmitted photons. Adapted from [51].*

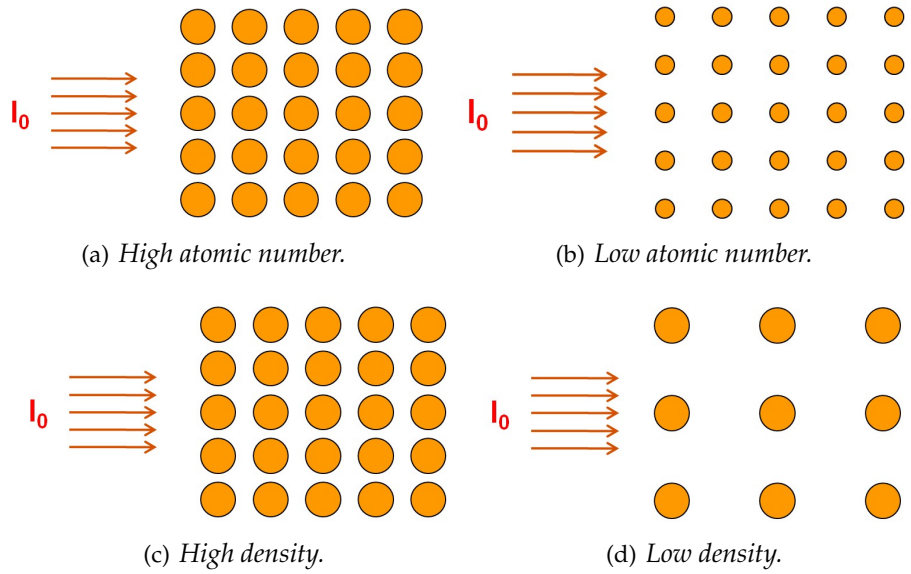


(a) *High atomic number.* (b) *Low atomic number.*

(c) *High density.* (d) *Low density.*

Figure 4.30: *A schematic picture of the influence of atomic number and density of material on transmitted X-ray photons intensity.*

More about penetration of the X-rays in different materials will be presented in Section 4.3.4.

Furthermore, penetration is directly connected to the object's geometry and dimensions

and therefore, the geometry and dimensions of the scanned object is presented in this section. The geometry and the thickness of the part have an important influence in the quantity of radiation absorbed by the part. It was mentioned earlier that complex geometries can be scanned using CT. For instance, a variation in the objects thickness is an important parameter for correct image reconstruction and prediction of the uncertainty. In order to analyze material-specific absorption and to adjust measurement parameters, reference objects, such as calibrated step cylinders, are used. Here, the measurands are the diameters and in particular, the cylinder form deviations. A strong gradient of the form deviation indicates the maximum material thickness that can be measured with a given CT system. Due to the energy-dependent absorption of X-rays, the low energy part of the X-ray spectrum is absorbed in the object much more than the high energy part [17]. This behavior is called beam hardening and is in details described in Section 4.3.2.

### 4.3.2 Beam hardening

#### State of the art and theoretical analysis

The X-ray beam traversing the matter consists of X-rays with a spectrum of different energies. Polychromatic X-ray beams with the lowest energies are preferentially absorbed, as the linear attenuation coefficient generally decreases with increasing energy. As a consequence, only X-rays with higher energies remain in the beam when passing the matter. These X-rays are less likely to be attenuated. Also, the longer the X-ray paths through the object, the more low energy photons are absorbed, resulting in a more penetrating beam. In other words, the beam becomes harder, i.e. its mean energy increases, which explains why this is called "beam hardening". Hence, for polychromatic radiation, the total attenuation, given by the logarithm of the ratio of the incoming and the attenuated X-ray beam, is no longer a linear function of objects thickness. If this nonlinear beam hardening effect is not compensated, the reconstructed images in X-ray CT will be corrupted by artifacts[1]: edge artifacts, streaks, and environmental artifacts [52–54]. Beam hardening makes it difficult to interpret the measured data quantitatively because it changes the attenuation. This complicates the threshold determination (workpiece surface) and the measurements of density and resolution. Consequently, higher measurement errors are expected if no beam hardening correction is applied. Furthermore, the same materials can result in different gray values depending on the surrounding material, which is known as the environmental density distortion [19, 32]. A typical picture of a beam hardening problem can be seen in Figure 4.31.

Beam hardening artifacts can however be reduced, or even completely eliminated. The reduction of beam hardening effect is done by:

- Pre-hardening of the beam using a filter (aluminum, copper or brass) (this was discussed in Section 4.1.1)
- Using smaller samples
- Correction during image reconstruction

[1] An artifact is something in an image that does not correspond to a physical feature in the test object. All imaging systems, whether CT or conventional radiography, exhibit artifacts.

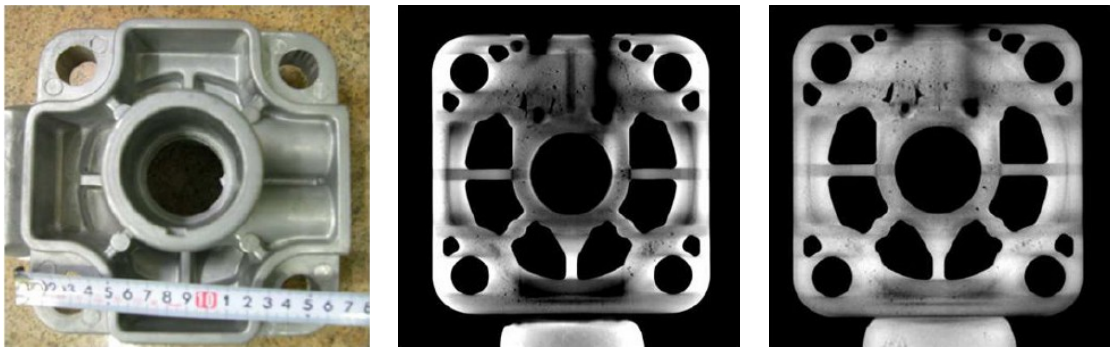

(a) *Aluminum casting.* (b) *A slice of the 225kV cone beam CT scan.* (c) *A slice of the 450kV cone beam CT scan.*

Figure 4.31: *Beam hardening effect - Artefacts due to lack of penetration [55].*

**Linearization**
Linearization technique evaluated by Herman [56] is one of the methods to reduce beam hardening effect in mono-material objects. This technique is based on the estimation of the relation between a propagated path length within the specimen and an according measured weakened intensity by means of various estimation algorithms. The resulting characteristic line can be used to compute beam hardening corrected intensity values which allow the reconstruction of an artifact free CT image. The characteristic line can be determined by performing a reference measurement using a reference object, e.g. a step wedge 4.32. This step wedge has to be composed of the same material as the specimen. Furthermore, the reference measurement has to be performed for each CT scan under the same conditions (current, voltage, trajectory, material, etc.) like for the specimen itself. Alternatively, the characteristic line can be determined out of the reconstructed CT image itself. For this purpose, a binarization is performed on the CT image. The path lengths within the binarized CT image are computed with a ray tracing algorithm and assigned to corresponding measured intensities. The resulting data point cloud is approximated by a fitting routine and yields the characteristic line. This method has the advantage that no reference measurement is needed and works fine for almost every homogeneous object [40].

**IAR method**
The Iterative Artifact Reduction (IAR) method is an iterative process where several post-processing steps are applied to the reconstructed volume in order to calculate a beam hardening correction independently of any reference object. The IAR process includes a model for estimating scattering called Length Based Scattering Approximation (LBSA). The IAR method requires the projection (raw) data and currently works only for homogeneous specimens. Figure 4.33 displays the impact of the IAR correction on the quality of CT data [27].

To avoid the beam hardening effect totally, monochromatic radiation is used. Such radiation is provided by synchrotron and is sometimes called ”synchrotron radiation”. Figure 4.34 show the principal of monochromatic radiation, schematic working principal of synchrotron and an example of a real synchrotron facility.

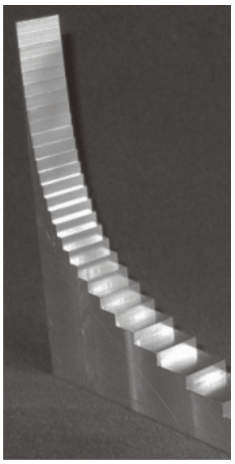

Figure 4.32: *Step wedge [57].*

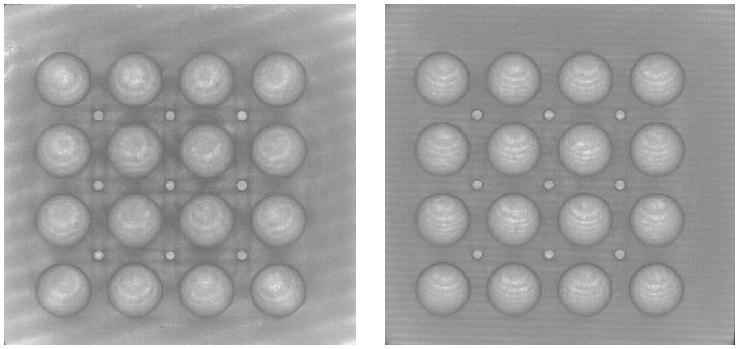

(a) *No correction applied.* (b) *IAR correction method applied.*

Figure 4.33: *IAR correction method applied on a ball calotte plate in order to reduce beam hardening effect [27].*

The importance of the problem of correcting/avoiding of beam hardening effect in CT is reported in many research publications [20, 27, 37, 41, 55, 59–61]. Below, a brief summary of methods for beam hardening correction is presented along with their advantages and disadvantages.

### 4.3.3 Scattered radiation

#### State of the art and theoretical analysis

According to [35], scatter is redirection of radiation beam photons due to interactions with matter in their path. Photons of the penetrating radiation used in tomography can interact with the electrons in a material in a manner which changes the direction of the photon. This scattering process has several implications for tomographic measurements:

1. The photon will generally not interact in the detector toward which it was originally traveling (causing attenuation of the primary beam)

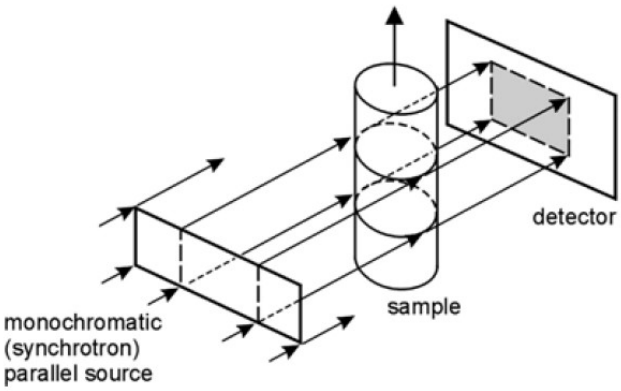


(a) *Principal of monochromatic radiation.*

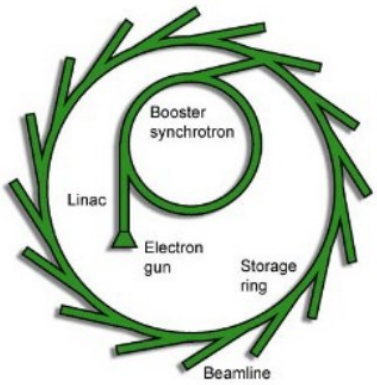


(b) *Schematic view on synchrotron working principle.*

(c) *Diamond Light Source - UK's national synchrotron science facility in Oxfordshire.*

Figure 4.34: *Synchrotron radiation - monochromatic X-ray source [58].*

2. The photon will usually transfer some of its energy to an electron in the material (causing dose in the object or signal in the detector)

3. Such a scattered photon may interact some detector not on its original path (introducing error into the associated opacity measurement)

The contribution of scattered photons to measurements may be greatly reduced, but not completely eliminated, in some cases by collimation of the detector array or separation of the detector from the object; it is sometimes compensated for by subtracting an estimate of its value from the measurements [35]. Several algorithms exist to reduce the effect of the scatter. These algorithms can also be reduced by proper thresholding.

Values of scatter and of X-ray attenuation due to scatter can be found in [62].

### 4.3.4 Material composition

**State of the art and theoretical analysis**

The material composition will mainly determine the energy-dependent absorption (beam hardening), obtaining better results for materials absorbing less radiation (for example plastics). If the measured part is composed by a diversity of materials, unexpected and important effects can be obtained.

In CT, objects of almost all material composition can be scanned. Anyhow, among typical materials in CT belong steels, polymers, ceramics, titanium, ruby and composite materials. The measurement object must be sufficiently penetrable for X-rays to pass through. For different materials, different linear attenuation coefficients (see Table 4.4) exist and moreover, depending on the material density, each material absorbs the X-rays differently. Therefore, influence from the material chosen prior the scanning plays a big role. Especially, when scanning multi-material components, severe streaking artifacts are introduced due to major changes in attenuation from one projection to the next. A graph of an example for maximum material penetration of the X-rays through the matter of iron (Fe) and aluminum (Al) at 420 keV can be seen in Figure 4.35.

Table 4.4: Linear attenuation coefficient, $\mu$ [mm$^{-1}$], of selected materials.

| **Material** | **Energy** | | | |
|---|---|---|---|---|
| | 40keV | 50keV | 60keV | 80keV |
| Gold (Au) | 25.1 | 14 | 8.75 | 4.22 |
| Lead (Pb) | 16.3 | 9.11 | 5.69 | 2.74 |
| Copper (Cu) | 4.36 | 2.34 | 1.43 | 0.684 |
| Nickel (Ni) | 4.09 | 2.2 | 1.35 | 0.65 |
| Aluminum (Al) | 0.154 | 0.0995 | 0.0751 | 0.0545 |
| Borosilicate glass | 0.109 | 0.0759 | 0.0607 | 0.0474 |
| PTFE (Teflon) | 0.0577 | 0.0465 | 0.041 | 0.0356 |

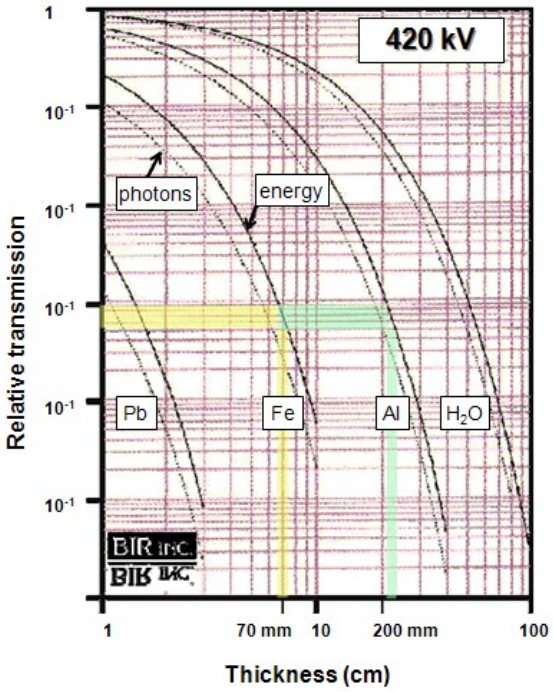


Figure 4.35: *Maximum allowable penetration of the X-rays at 420 keV for Fe and Al [29].*

### 4.3.5 Surface roughness

#### State of the art and theoretical analysis

Surface of the real objects is not perfect and therefore results in difficulties for threshold value determination. The quantification of the uncertainty caused by surface roughness is currently under development. In [63], the uncertainty due to the surface roughness was assessed as:

$$u_{\mathrm{wi}} = \sqrt{\left(\frac{b \cdot Rz_{\mathrm{mean}}}{2}\right)^2} \tag{4.8}$$

Here, the influence of the surface structure was determined by measuring the roughness at various spots on the workpiece surface. The mean value from this measurement, $Rz_{\mathrm{mean}}$, was assumed as representative for the whole workpiece. The generation of the surface after the tomographic imaging poses a low-pass filter with a spatial resolution of the voxel size. It is estimated that the generated surface lies half within the material of the part. While roughness peaks cause local shading, roughness valleys let pass more intensity. As the pixel size ($400\ \mu m$) is comparatively bigger than the roughness, only an average shift of the surface point is detected after segmentation. This means that the error margin is half of $Rz_{\mathrm{mean}}$. For the standard uncertainty based on error margins a rectangular distribution with the factor *b=0.6* is assumed.

## 4.4 Environment

Temperature, humidity and vibration are the most relevant influence factors, because they may influence the acquired data by adding further noise. Filtration in this case is necessary so that unwanted data can be eliminated for further 3D reconstruction. Not many studies on influence of environment in CT are documented so far. An experimental investigation on influence of temperature on stability of target material (Mo) is presented in [64]. As explained in Section 4.1.1, heat is generated at the target material and also from coils used for moving and focusing electrons. To reduce stability problems due to temperature changes of the system and the sample, an additional X-ray tube-cooling (from GE/Phoenix|x-ray) was installed. The results show that the maximum temperature at the target is lower when the cooling is applied and the temperature stabilizes after 25 minutes, see Figure 4.36.

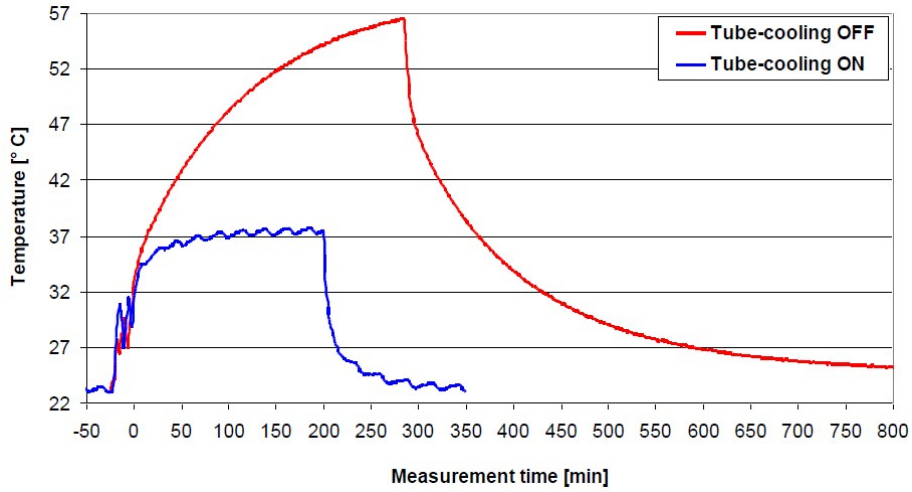


Figure 4.36: *Temperature influence on stability of target material in Nanotom CT scanner [64].*

## 4.5 Operator

The operator has practically no direct influence on the CT measurement results. However, measuring strategy and its implementation is a matter of the experience of the operator and moreover, there are parameters that need to be set prior scanning and thus the user's experience plays a crucial role in setting up the program for CT measurement. Process parameters like magnification, orientation of the measurement object, energy of the X-ray source (source current and acceleration voltage), detector integration time, etc. are necessary for correct data processing and image reconstruction. Therefore, these influence quantities has to be analyzed so that a measurement uncertainty of observed deviations based on the user impact can be assessed.

### 4.5.1 Magnification

**State of the art and theoretical analysis**

The resulting voxel size *VS* influences the resolution of a CT system. The VS depends on the geometrical magnification, *M*, the pixel to pixel distance, $d_{\text{det}}$, of the detector and the diameter, $d_{\text{s}}$, of the X-ray source. The magnification can be expressed as follows:

$$M = \frac{FDD}{FOD} \tag{4.9}$$

where *FDD* is a distance between focus and detector and *FOD* is a distance between focus and object. Figure 4.37 shows that the magnification can be increased by moving the sample closer to the X-ray source and vice versa. In the ideal case, one obtain small voxel size (higher magnification and resolution) by choosing a low value of *FOD* or a high value of *FDD* and thus a large geometrical magnification. Voxel size is then only determined by the pixel to pixel distance of the detector and the magnification [16] resulting in the following equation:

$$VS = \frac{d_{\text{det}}}{M} \tag{4.10}$$

In order to make an accurate reconstruction of the volumetric data, the entire sample must remain within the field of view, *FOV*, and cone beam during the rotation. The maximum magnification is limited by the ratio of the effective detector width, *D*, and the sample diameter, *d*, and can be expressed as:

$$M = \frac{D}{d} \tag{4.11}$$

When short measurement times are required, lower magnifications are chosen to image the part entirely on the detector during a single measurement cycle. By scanning selected ROI, small features in large parts can be measured and increase in resolution can be achieved [60] (see Figure 4.38).

A limit for the resolution in CT is the size and the shape of the X-ray focus. For X-ray tubes the minimum focus size increases with tube power and tube voltage. For larger parts, tubes of higher voltage have to be employed. Therefore, the achievable resolution deteriorates with the size of the scanned object [19]. The influence of the spot size on the image blurring is shown in Figure 4.4 in Section 4.1.1.

**Experimental investigation**

An experimental investigation on influence of magnification was performed using replica step gauge and since this investigation also concerned workpiece positioning and orientation, it is presented in Section 4.5.2.

Another study on workpiece orientation was performed in [48], but since this investigation also concerns influence of the number of projections, it is presented in Section 4.5.3.

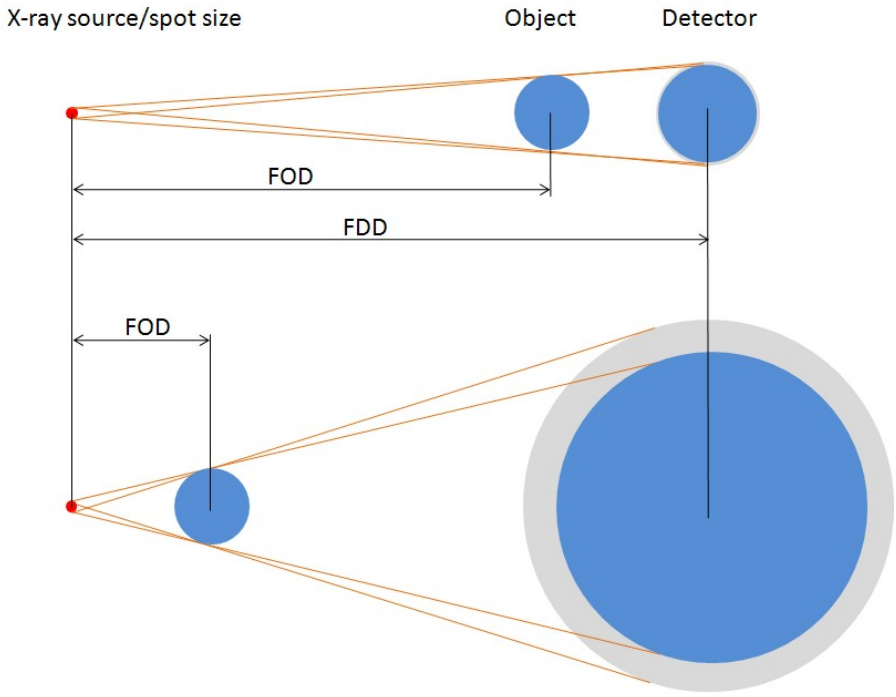


Figure 4.37: *Influence of magnification and blurring effect (penumbra) caused due to the spot size. Small magnification obtained when moving the object further from the X-ray source (top) and high magnification obtained when moving the object closer to the X-ray source (bottom).*

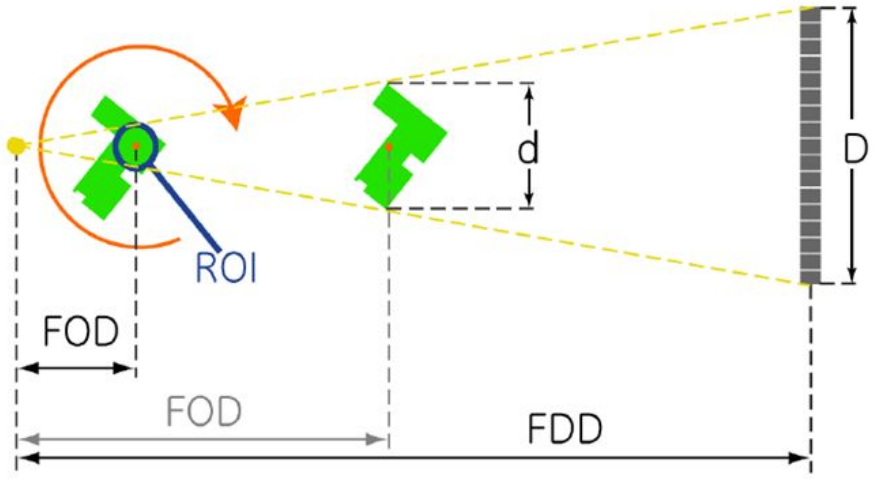


Figure 4.38: *CT setup for a cone beam [Source: Phoenix|x-ray].*

### 4.5.2 Workpiece positioning and orientation

#### State of the art and theoretical analysis

The workpiece is positioned and fixed on the rotary table so that it does not move or turn while scanning. The orientation of the measurement object influences the variation

of the length of the way the rays pass through the object during the rotation while the object is being measured. In bigger variation of the length of the object (as it occurs when there are big variations of workpiece sections during acquisition) one can expect weak and improper image reconstruction, because of not-correct exposure of reconstructed projections. Some images can be outshined and others too dark because of different lengths of X-rays [48]. Both situations have to be avoided and well exposed projections are required for a proper reconstruction of the volumetric model. If this is not achieved, artefacts caused by wobbling occur on the volumetric model. Therefore, the user positions the scanned object, if possible, in the way that the length the rays travel through the object is equally distributed along all angle positions.

It was reported in [60] that for simple geometries like hollow cylinders, the influence of the object position on the rotary table is not important as for real complex shaped objects.

**Experimental investigation**

The authors performed an investigation concerning influence of workpiece orientation, magnification, source-object-detector distance and surface extraction method on performances of a CT scanner. A 42 mm replica step gauge used for optical scanner verification [65, 66] was used to evaluate accuracy of a Nanotom®CT scanner from GE Phoenix|X-ray, situated at Novo Nordisk®. Experimental tests were performed orienting the workpiece in two directions, vertical and at 45°, as shown in Figure 4.39. Accuracy of the CT system was evaluated computing the error of indication for size measurement, $E$, as suggested in the VDI/VDE 2617-6.2 [67].

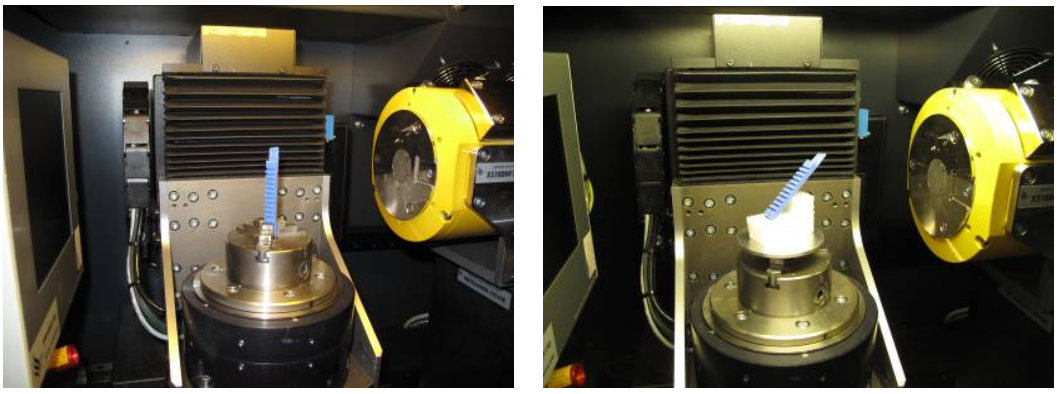

(a) *Vertical position.* (b) *45° with respect to the rotation axis.*

Figure 4.39: *Orientation of the step gauge in the scanning volume.*

According to the standard, the error of indication for size measurement can be computed either through a bidirectional path or a unidirectional one. In latter, it is necessary to correct it by adding the probing errors (probing error form, *PF*, and probing error size, *PS*). *PS* and *PF* are usually computed using spheres (ball bars, ball plates). In the following, the list of computed parameters is reported:

- *PF*: probing error found in the ball bar spheres

- $PS$: calculated error in the diameter of the ball bar spheres
- $E$: error for size measurement
- $L_{\mathrm{M}}$: measured distance between two teeth side of the step gauge (on the scans)
- $L_{\mathrm{C}}$: calibrated distance between two teeth side of the step gauge (with the CMM)

Probing errors were evaluated using the ball bar. Error of indication for size measurement was computed using the replica step gauge by applying a unidirectional strategy. For more details see [67].

The characteristic probing error form, $PF$, is the range of radial deviations between the measurements points and the calculated regression sphere. This is identical to the difference between the maximum $R_{\mathrm{max}}$ and minimum $R_{\mathrm{min}}$ distances of probing points from the center of the regression sphere (see Figure 4.40(a)). The probing error of form measurement is expressed in Equation 4.12. Probing error size, $PS$, is determined from the difference between the measured $D_{\mathrm{M}}$ and calibrated $D_{\mathrm{r}}$ diameters of the reference sphere (see Figure 4.40(b)). The probing error of size measurement is expressed in Equation 4.13.

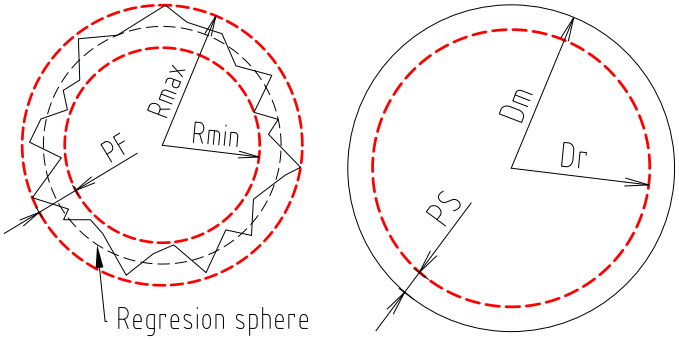


(a) *Probing error form, PF.* (b) *Probing error size, PS.*

Figure 4.40: *Definition of probing errors.*

$$PF = R_{\mathrm{max}} - R_{\mathrm{min}} \tag{4.12}$$

$$PS = D_{\mathrm{m}} - D_{\mathrm{r}} \tag{4.13}$$

$$E_{\mathrm{unidirectional}} = L_{\mathrm{M}} - L_{\mathrm{C}} + PS \pm PF \tag{4.14}$$

Four incremental distances on the step gauge grooves were measured unidirectionally. The overall $E$ was computed as the maximum absolute value of the four obtained distances for each setup. Reference measurements were taken using a tactile CMM. Having the step gauge mounted vertically, three setups were considered: two with the same magnification, corresponding to a voxel size $(s) = 20\ \mu m$ and the third setup applying magnification, corresponding to a $s = 30\ \mu m$. In the two cases with the same magnification, different distances between the X-ray source and the detector were chosen

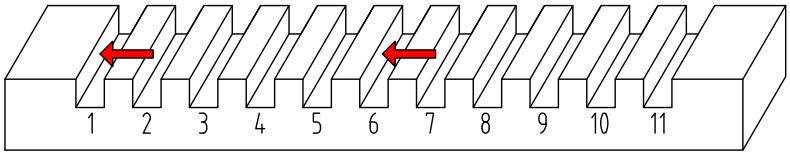


Figure 4.41: *Example of unidirectional measurement between groove 1 and groove 6 using step gauge.*

(FDD parameter, see Table 4.5). In the first case the detector was closer to the X-ray source and in the second case farther from the X-ray source. The other parameter considered was the threshold technique applied to extract the surface (global and local thresholding method).

Errors of indication for size measurement, $E$, in the considered setups are reported in Figure 4.42. Results show that the higher magnification does not assure the best accuracy. This is due to two effects: (1) in the first instance, noise at the borders of the step gauge is present because of interaction between the X-ray cone beam source and straight surfaces perpendicular to the rotation axis. The effect is more severe when the incidence angle is bigger (i.e. workpiece and X-ray source are closer), even if the same magnification (voxel size) is chosen. (2) Another effect is introduced due to blurring. As the workpiece is moved closer to the X-ray source (higher magnification), more blurred images will be obtained because of the finite dimension of the X-ray spot size, see Figure 4.37. Both effects were also pointed out in [38]. Concerning surface extraction, results obtained with local thresholding are generally more accurate than with global thresholding. Only in Setup 1, $E$ values obtained with global threshold were sometimes better. This could be due to amplification of local noise that takes place with local thresholding, as it can be seen on the CT scans for Setup 1.

Further tests were accomplished by positioning the step gauge tilted 45° with respect to the rotation axis of the scanner. A comparison to results obtained with the step gauge positioned vertically for the first two setups (same magnification) was made. All results (see Figure 4.43) show that by positioning the step gauge at 45° it is possible to improve values of $E$ by more than 50% with respect to the vertical position, because of a significant reduction of border noise on the flat surfaces of the steps.

Optimization of positioning of a workpiece in the CT scanner cabinet is important to enhance accuracy of CT measurements. Influences of the workpiece orientation, system magnification, source-object-detector distances and surface extraction method on an industrial CT scanner performance were evaluated using a replica step gauge, already used for optical scanner verification. Results show that the position of the workpiece in the measuring volume is fundamental to obtain reliable measurements. Important improvements of accuracy are obtained by positioning the workpiece at 45° with respect to the rotation axis.

Table 4.5: Parameter setup for experiments.

| Parameter | Setup 1 | Setup 2 | Setup 3 |
|---|---|---|---|
| Magnification | 2.5 | 2.5 | 1.667 |
| *FDD* [mm] | 275 | 500 | 500 |
| $s$ [$\mu m$] | 20 | 20 | 30 |

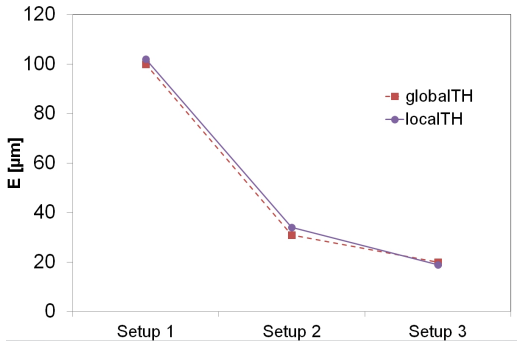


Figure 4.42: *Errors of indication for size measurements with step gauge positioned vertically by applying global and local thresholding.*

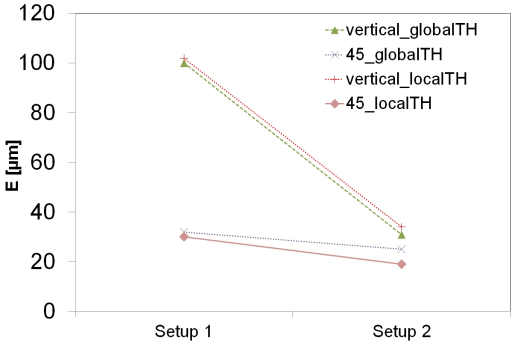


Figure 4.43: *Comparison of results for Setup 1 and Setup 2 with the step gauge positioned vertical and 45° by applying global and local thresholding.*

### 4.5.3 Number of projections

#### State of the art and theoretical analysis

The number of projections (angle positions) is directly connected with scanning time and data acquisition time and therefore, it is of the industrial interest to reduce the number of projections to minimum for speeding up the scanning process. In this way, the associated cost can be efficiently reduced.

#### Experimental investigation

It was shown in [48] that number of projections does not play a vital role in connection with resulting image quality and therefore belong to less important uncertainty contributors. A bigger amount of projections within one revolution of the scanned object increases the quality of the reconstructed data set but increases the necessary measurement time. As more than 800 projections reduce the deviations by less than 5% it seems sufficient to use 400-800 projections for accurate reconstruction of the object. A four factor experimental design at two levels was built (see Table 4.6), evaluating the diameter of a cylinder made of different materials (Aluminum, PMMA and PVC). Results presented in Figure 4.44 show that the threshold is the most important influence parameter. Also magnification and orientation of the workpiece have a significant effect. The least important is the number of projection, as discussed in 4.5.3.

Table 4.6: Factor settings for evaluation of measurements [48].

| | Settings | |
|---|---|---|
| **Factor** | - | + |
| Magnification | 1x | 2x |
| Orientation | parallel to rotation axis | perpendicular to rotation axis |
| Number of projections | 400 | 1600 |
| Threshold method | global | local adaptive |

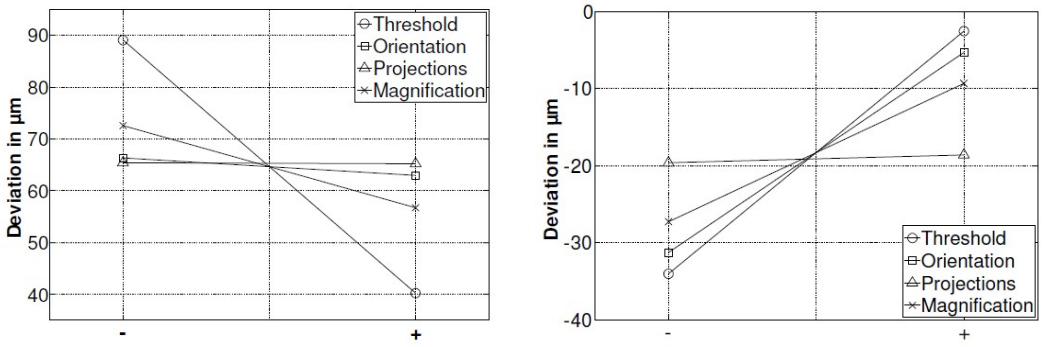


(a) *Results for outer diameter.* (b) *Results for outer diameter.*

Figure 4.44: *Influence of threshold method, object orientation, number of projections and magnification on measurements of diameter of the hollow cylinder made of PVC [48].*

### 4.5.4 Detector exposure time

#### State of the art and theoretical analysis

The total time for to perform a CT scan depends on different factors, like number of projections, number of skipped images and the detector exposure (or integration) time. By increasing the detector exposure time, the scanning time increases but the image noise is reduced [68]. The number of remaining X-ray photons reaching a single detector element increases with the increase of integration time [69].

# Chapter 5

# Conclusion

This report focuses on CT applications for industrial and metrological purposes, where attention is on the current challenges in CT, i.e. establishment of traceability and uncertainty assessment. A complete overview of factors influencing CT accuracy is described in details. A thorough review of the state of the art, a theoretical analysis and an experimental investigation in order to assess the influence of reference, instrument, workpiece, environment and procedure on the precision and traceability of measurement results from CT, is realized. In particular, experimental investigations concern methods and techniques to correct and reduce errors and artefacts due to a defined parameter, both as they can be found in literature and performed by the authors.

# References


[1] W. A. Kalender, X-ray computed tomography, Physics in Medicine & Biology **51** (2006) 29–43.

[2] C. Reinhart, C. Poliwoda, T. Guenther, W. Roemer, S. Maas, C. Gosch, Modern voxel based data and geometry analysis software tools for industrial CT, Proceedings of the 16th World Conference on NDT, Montreal, Canada (2004) 8.

[3] http://en.wikipedia.org/wiki/wilhelm_conrad_r%c3%b6ntgen (read 18/01/2011).

[4] http://www.aps.org/publications/apsnews/200411/history.cfm (read 18/01/2011).

[5] http://en.wikipedia.org/wiki/godfrey_hounsfield (read 18/01/2011).

[6] M. Willcox, G. Downes, A brief description of NDT techniques, Insight NDT technical paper (2003) 1–22.

[7] B. P. C. Rao, Non-Destructive evaluation (NDE), http://web.archive.org/web/20091026221654/www.geocities.com/raobpc/index.html (read 18/01/2011).

[8] A. R. Ganesan, Holographic and laser speckle methods in non-destructive testing, Proceedings of the National Seminar and Exhibition on Non-destructive Evaluation (2009) 5.

[9] Non-Destructive Testing of materials, http://ieo.dit.ie/technical_ndt.html (read 18/01/2011).

[10] Optical holography for surface deformation, http://www.dashinspectorate.com/blog (read 18/01/2011).

[11] G. Reynolds, D. Servaes, L. Ramos-Izquierdo, J. BeVelis, D. Peirce, P. Hilton, R. Mayville, Holographic fringe linearization interferometry for defect detection, Optical Engineering **24** (5) (1985) 757–768.

[12] W. Hossack, Modern optics: Lecture notes, http://www2.ph.ed.ac.uk/ wjh/teaching/mo (read 18/01/2011).

[13] P. Mix, Introduction to non-destructive testing: A training guide, 2nd Edition (2005) ISBN: 978–0–471–42029–3.

[14] M. Honlet, Nondestructive testing of complex composite materials and structures using optical techniques, Abstracts of the 1997 COFREND Congress on Nondestructive Testing, Nantes, France (1997) 6.

[15] Nondestructive testing of complex composite materials and structures using optical techniques, Advanced Materials & Processes **166** (2008) 39–48.

[16] R. B. Bergmann, F. T. Bessler, W. Bauer, Computer tomography for nondestructive testing in the automotive industry, Proceedings of SPIE **5535** (1) (2004) 464–472.

[17] M. Bartscher, U. Hilpert, J. Goebbels, G. Weidemann, Enhancement and proof of accuracy of industrial computed tomography (ct) measurements, Annals of CIRP **56** (1) (2007) 495–498.

[18] VDI/VDE 2630 Sheet 1.2 - Computed tomography in dimensional measurement - Influencing variables on measurement results and recommendations for computed tomography dimensional measurements, VDI/VDE Society for Metrology and Automation Engineering (GMA) (2010).

[19] S. Carmignato, Traceability of dimensional measurements in computed tomography, In: Proceedings of 8th A.I.Te.M. Conference (2007) 11.

[20] M. Franz, C. Funk, J. Hiller, S. Kasperl, M. Krumm, S. Schröpfer, Reliability of dimensional measurements by computed tomography for industrial applications, 4th European-American Workshop on Reliability of NDE (2009) 8.

[21] A. Sasov, Comparison of fan-beam, cone-beam and spiral scan reconstruction in x-ray micro-ct, Proceedings of SPIE **4503** (2002) 124–131.

[22] D. Wildenschild, J. Hopmans, C. Vaz, M. Rivers, D. Rikard, B. Christensen, Using X-ray computed tomography in hydrology: systems, resolutions, and limitations, Journal of Hydrology **267** (2002) 285–297.

[23] J.-P. Kruth, Industrial application of ct scanning in engineering and manufacture, 14th CMM Danish users' club conference on 'Application of CT scanning in industry' (2010) Presentation slides.

[24] ISO 15708-1:2002 - Non-destructive testing - Radiation methods - Computed tomography: Part 1: principles.

[25] E. Neuser, A. Suppes, Visualizing internal 3D structures with submicrometer resolution, International Symposium on Digital industrial Radiology and Computed Tomography, Lyon, France (2007) 18.

[26] M. Bartscher, U. Neuschaefer-Rube, F. Wäldele, Computed tomography - A highly potential tool for industrial quality control and production near measurements, NUMB 1860 (2004) 477–482.

[27] S. Kasperl, J. Hiller, M. Krumm, Computed tomography metrology in industrial research and development, MP Materials Testing **51** (6) (2009) 405–411.

[28] O. Brunke, 3D Dimensional metrology with high resolution CT vs. tactile CMMs, High-Resolution X-ray CT Symposium, Dresden, Germany (2010) Presentation slides.

[29] 14th CMM Danish users' club conference on 'Application of CT scanning in industry', DTU (2010).

[30] S. Carmignato, Traceability of dimensional measurements from CT scanning, 14th CMM Danish users' club conference on 'Application of CT scanning in industry' (2010) Presentation slides.

[31] C. Reinhart, VG studio MAX: Application examples from science and industry, High-Resolution X-ray CT Symposium, Dresden, Germany (2010) Presentation slides.

[32] E. v. d. Casteele, Model-based approach for beam hardening correction and resolution measurements in microtomography, Ph.D. thesis, Universiteit Antwerpen (2004).

[33] M. Alexandru, A. Nistor, The Röntgen radiation and its application in studies of advanced materials, Physics of advanced materials winter school (2008) 18.

[34] J.R. Connolly, Introduction to X-ray powder diffraction: Lecture notes. http://epswww.unm.edu/xrd/xrd-course-info.htm (read 31/01/2011).

[35] ASTM E1441 - 00:2005. Standard guide for computed tomography (CT) imaging, Technical report.

[36] ISO 15708 - Non-destructive testing - Radiagraphic methods - Computer tomography - Part 1 - Principles, ISO International Standard (2002).

[37] R. Ketcham, W. Carlson, Acquisition, optimization and interpretation of x-ray computed tomographic imagery: applications to the geosciences, Computers & Geosciences **27** (2001) 381–400.

[38] F. Welkenhuyzen, K. Kiekens, M. Pierlet, W. Dewulf, P. Bleys, J.-P. Kruth, A. Voet, Industrial computer tomography for dimensional metrology: Overview of influence factors and improvement strategies, 4th International Conference on Optical Measurement Techniques for Structures and Systems (OPTIMESS2009), Antwerp, Belgium (2009) 9.

[39] K. Holt. X-ray production & emission. http://www.elcamino.edu/faculty/kholt/RT%20111%20presentations/X-Ray%20Production%20&%20Emission_W4.ppt (read 02/02/2011).

[40] M. Krumm, S. Karlson, M. Franz, Reducing non-linear artifacts of multi-material objects in industrial 3D computed tomography, NDT&E International **41** (2008) 242–251.

[41] J. Kastner, D. Heim, D. Salaberger, C. Sauerwein, M. Simon, H. Wälischmiller, Advanced applications of computed tomography by combining of different methods, Proceedings of 9th European Congress on Non-Destructive Testing (2006) 8.

[42] Y. Sun, Y. Hou, F. Zao, J. Hu, A calibration method for misaligned scanner geometry in cone-beam computed tomography, NDT&E International **39** (2006) 499–513.

[43] P. Wenig, S. Kasperl, Examination of the measurement uncertainty on dimensional measurements by x-ray computed tomography, Proceedings of 9th European Congress on Non-Destructive Testing, Berlin, Germany (2006) 10.

[44] J. Beutel, H. Kundel, R. van Metten, Handbook of medical imaging, Physics and Psychophysics **1** (2000) SPIE Press Monograph Vol. PM79.

[45] R. Hanke, T. Fuchs, N. Uhlmann, X-ray based methods for non-destructive testing and material characterization, Nuclear Instruments and Methods in Physics Research **591** (2008) 14–18.

[46] C. Reinhart, Industrial computer tomography - A universal inspection tool, 17th World Conference on Nondestructive Testing (WCNDT2008), Shanghai, China (2008) 10.

[47] H.-C. Saewert, D. Fiedler, M. Bartscher, F. Wäldele, Obtaining dimensional information by industrial CT scanning - present and prospective process chain, CT-IP (2003) 163–172.

[48] A. Weckenmann, P. T. Krämer, Predetermination of measurement uncertainty in the application of computed tomography, 11th CIRP International Conference on Computer Aided Tolerancing, Annecy, France (2009) 5.

[49] R. Sauro, Validation of CT scanners with investigation on CT data processing, M.Sc. thesis, Technical University of Denmark (2010).

[50] M. Bartscher, M. Neukamm, U. Hilpert, U. Neuschaefer-Rube, F. Härtig, K. Kniel, K. Ehrig, A. Staude, J. Goebbels, Achieving traceability of industrial computed tomography, Key Engineering Materials **437** (2010) 79–83.

[51] http://www.ndt-ed.org (read 15/02/2011).

[52] R. A. Brooks, G. D. Chiro, Beam hardening in X-ray reconstructive tomography, Physics in Medicine and Biology **21** (3) (1976) 390–398.

[53] R. F. D. Paiva, J. Lynch, E. Rosenberg, M. Bisiaux, The effect of beam hardening on resolution in X-ray microtomography, Nondestructive testing and evaluation **31** (1) (1998) 17–22.

[54] S. W. Young, , H. H. Müller, W. H. Marshall, Computed tomography: Beam hardening and environmental density artifact, Radiology **148** (1983) 279–283.

[55] M. Simon, I. Tiseanu, C. Sauerwein, S.-M. Yoo, I.-S. Cho, Development of multi sensor and multi source computed tomography systems, International Symposium on Digital industrial Radiology and Computed Tomography, Lyon, France (2009) 9.

[56] G. Herman, Correction for beam hardening in computed tomography, Physics in Medicine & Biology **21** (1) (1979) 81–106.

[57] J. Hiller, Seminar on industrial CT, Kgs. Lyngby, Denmark (2010) Presentation slides.

[58] Visiting the UK's largest particle accelerator.http://www.ianvisits.co.uk/blog/2010/11/14/visiting-the-uks-largest-particle-accelerator/ (read 21/01/2011).

[59] C. Heinzl, J. Kastner, T. Möller, , M. Gröller, Statistical analysis of multi-material components using dual energy ct, Vision, Modeling and Visualization (VMV), Konstanz, Germany (2008) 179–188.

[60] T. Paul, Z. He, Advanced NDT with high resolution computed tomography, 17th World Conference on Nondestructive Testing (WCNDT2008), Shanghai, China (2008) 9.

[61] O. Brunke, K. Brockdorf, S. Drews, B. Müller, T. Donath, J. Herzen, F. Beckmann, Comparison between x-ray tube based and synchrotron radiation based $\mu$ct, Proceedings of SPIE 7078 (2008) 12.

[62] J.H. Hubbell and S.M. Seltzer, Tables of X-ray mass attenuation coefficients and mass energy-absorption coefficients from 1keV to 20MeV for elements Z=1 to 92 and 48 additional substances of dosimetric interest. http://www.nist.gov/pml/data/xraycoef/index.cfm (read 28/02/2011).

[63] R. Schmitt, C. Niggemann, Uncertainty in measurement for x-ray-computed tomography using calibrated workpieces, Measuring Science & Technology **21** (2010) 1–9.

[64] D. Salaberger, B. Plank, J. Kastner, B. Harrer, G. Requena, H.-P. Degischer, O. Brunke, Comparative study of high resolution cone beam X-ray computed tomography methods and discussion of temperature influence on Nanotom stability, High-Resolution X-ray CT Symposium, Dresden, Germany (2010) Presentation slides.

[65] L. D. Chiffre, S. Carmignato, A. Cantatore, J. Jensen, Replica calibration artefacts for optical 3d scanning of micro parts, Proceedings of the 9th Euspen International Conference, San Sebastian, Spain (2009) 352–355.

[66] A. Cantatore, L. D. Chiffre, S. Carmignato, Investigation on a replica step gauge for optical 3d scanning of micro parts, Proceedings of the 10th Euspen International Conference - Delft, Netherlands (2010) 200–203.

[67] VDI/VDE 2617 - Part 6.2: Accuracy of coordinate measuring machines - Characteristics and their testing - Guideline for the application of DIN EN ISO 10360 to coordinate measuring machines with optical sensors, VDI/VDE-Gesellschaft Mess- und Automatisierungstechnik (GMA) (2005).

[68] M. Reiter, C. Heinzl, D. Salamberger, D. Weiss, J. Kastner, Study on parameter variation of an industrial computed tomography simulation tool concerning dimensional measurements devations, 10th European conference on non-destructive testing (ECNDT), Moscow, Russia (2010) 10.

[69] U. Hassler, S. Oeckl, I. Bauscher, Inline ct methods for industrial production, International Symposium on NDT in Aerspace, Fürth, Germany (2008) 8.